



Challenges of initial Thorium and Approaches to Robust Speleothem Age Models: A case study from the Yucatán peninsula, Mexico

Nils Schorndorf^{1,2}, Sophie F. Warken^{1,2*}, René Eichstädter^{1†}, Aaron S. Mielke^{1,2}, Jerónimo Avilés Olguín^{3,4}, Frank Keppler², Dominik Hennhöfer⁵, Fátima Tec Pool⁴, Carlos Evia⁴, María José Gómez⁴,
5 Wolfgang Stinnesbeck² and Norbert Frank^{1,2*}

¹Institute of Environmental Physics, Heidelberg University, Heidelberg, 69120 Heidelberg, Germany

²Institute of Earth Sciences, Heidelberg University, Heidelberg, 69120 Heidelberg, Germany

³Museo del Desierto, Saltillo 25022, Coahuila, Mexico

⁴Grupo Espeleológico Ajau, Merida, Yucatán, Mexico

10 ⁵Hessisches Landesmuseum Darmstadt, Friedensplatz 1, 64283 Darmstadt, Germany

† deceased

*Correspondence to: Sophie Warken (sophie.warken@uni-heidelberg.de)

Abstract. Speleothems, such as stalagmites and flowstones, are invaluable archives of past environmental and climatic conditions due to their layered growth and suitability for precise ²³⁰Th/U dating. These natural formations record hydroclimatic variability over time, offering insights into how environmental changes have influenced ecosystems and human societies. In the context of Mesoamerica, speleothem records provide an opportunity to explore potential links between climate variability and sociopolitical transformations during Maya cultural evolution. Paleoclimate archives from this region document severe dry conditions during the Terminal Classic Period (~800–1000 AD), a time marked by societal decline and urban abandonment among the Maya. Yet, existing records often suffer from limited
15 chronological precision, and high-resolution multi-proxy datasets from the area remain scarce. This study presents extensive ²³⁰Th/U dating of several speleothems from Áaktun Kóopo Cave, Yucatán, revealing continuous carbonate deposition over the past 2.7 kyr, encompassing the entire era of Maya cultural evolution, as well as evidence of speleothem growth during earlier glacial and interglacial periods. High uranium concentrations in the speleothems (averaging 1 ppm) enabled precise dating, despite challenges from elevated and variable detrital thorium contamination.
20 These challenges were addressed by combining multiple techniques, including isochron analysis, stratigraphic approaches, and annual layer counting, to constrain elevated and initial (²³⁰Th/²³²Th) activity ratios. Notably, we infer a high and largely unsystematic variability of high initial (²³⁰Th/²³²Th) activity ratios in space and time, with values spanning between 4 and 68. Still, our approach yields stalagmite chronologies from Áaktun Kóopo Cave that provide a robust foundation for detailed multi-proxy reconstructions of hydroclimate and vegetation changes over the past 2.7 kyr.
25 These chronologies address a critical gap in high-resolution data for this region and enable future studies to better resolve environmental conditions throughout Maya history.
30



1 Introduction

Reconstructing past environmental and climatic variability relies on archives that combine continuity, sensitivity to climate, and robust dating methods. Speleothems fulfil these criteria, as their layered carbonate growth can be precisely dated using U-series disequilibrium dating (Wendt et al., 2021; Scholz and Hoffmann, 2008; Cheng et al., 2013). Constructing accurate age models based on a large number of individual $^{230}\text{Th}/\text{U}$ ages is fundamental for interpreting speleothem climate proxy records, as chronological uncertainties directly affect the absolute timing of events, its duration, and partially the magnitude (smoothing) of inferred climate variability (Comas-Bru et al., 2020; Moseley et al., 2016). However, $^{230}\text{Th}/\text{U}$ dating assumes a closed system for the exchange of Uranium and its decay products upon speleothem formation, and it further presumes absence of initial ^{230}Th . In such an ideal theoretical scenario the Th/U age precision and accuracy will solely depend on the analytical precision and accuracy of isotope ratio measurements and isotope half-lives (Cheng et al., 2013). Any deviation of the carbonate precipitating environment from this ideal scenario may influence the age accuracy, either through U-series system opening via dissolution and reprecipitation of carbonate, or via a variable degree of initial Th contamination. To date, U-series system opening cannot be corrected for cave deposits due to the lack of constant boundary conditions such as a time-invariant U-isotope composition of drip water. Such U-series open system models only exist for well-preserved marine carbonates and assume a near constancy of seawater U-isotope ratios as additional constraint (Frank et al., 2006). For the presence of initial ^{230}Th , however, several strategies exist to correct for its influence. In most cases ^{230}Th is related to the detrital origin of ^{232}Th assuming a constant detrital activity ratio for linear correction models applied to the measured $^{230}\text{Th}/^{238}\text{U}$ activity ratio. Appropriate correction techniques have to be applied, which are, however, associated with relatively large uncertainties. Consequently, high Th contamination and young ages of speleothems result in $^{230}\text{Th}/\text{U}$ -age errors exceeding analytical precision by orders of magnitude (Ludwig and Titterton, 1994). This issue is particularly problematic for speleothems with low uranium concentrations and visible non-carbonate traces, since even small amounts of initial Th can lead to erroneously old age estimates (e.g., Faraji et al., 2023; Kerber et al., 2025; Fensterer et al., 2010).

A primary challenge with initial Th correction arises from the difficulty in accurately estimating the initial ($^{230}\text{Th}/^{232}\text{Th}$) activity ratio of detrital material (further on referred to as R02i), which can vary depending on the characteristics of the host rock, soil, and chemical complexing agents during aqueous transport of Th (Ivanovich and Harmon, 1992). For geological material in ^{238}U - ^{234}U - ^{230}Th secular equilibrium, and assuming a crustal $^{232}\text{Th}/^{238}\text{U}$ activity ratio of 3.8 (Taylor and McLennan, 1985), the resulting atomic $^{230}\text{Th}/^{232}\text{Th}$ ratio is $4.4 \pm 2.2 \times 10^{-6}$ (with an assumed error of 50%), equivalent to an activity ratio of ~ 0.8 . This ratio, widely utilized for detrital



²³⁰Th correction (Spötl et al., 2002), is commonly often applied to estimate initial ²³⁰Th and correct ²³⁰Th/U ages. This is particularly effective when absolute ²³²Th concentrations are low (< a few ng) and speleothems are older than several thousand years. However, tropical karst systems frequently exhibit elevated and variable R02i in drip waters, modern carbonates, and speleothems – sometimes up to 80 times higher than the commonly assumed value of ~ 0.8 for the upper continental crust. For example, speleothem studies from the Bahamas report a wide range of R02i between 2.2 to 18.7 (Beck et al., 2001; Arienzo et al., 2015; Hoffmann et al., 2010; Richards and Dorale, 2003). R02i ranging from 8 to 41 have been used to correct a Belizean stalagmite (Ridley et al., 2015), and values between 11 and 61 were applied to Puerto Rican stalagmites (Kerber et al., 2025; Vieten et al., 2024a; Vieten et al., 2024b; Warken et al., 2020; Rivera-Collazo et al., 2015). Also at other sites including Cuba (Fensterer et al., 2010), Mexico (Moseley et al., 2015; Kennett et al., 2022; Stinnesbeck et al., 2020) or in the tropical Pacific (Faraji et al., 2021; Partin et al., 2007; Carolin et al., 2013) elevated R02i were found. These observations underscore the necessity of addressing variability in initial Th activity ratios when correcting ²³⁰Th/U ages from such environments. In general, there are two main approaches to assess R02i in speleothems: (1) direct measurement of the contaminating phase, e.g., from cave drip water, soil, or zero-age carbonate (ZAC) (Kerber et al., 2025; Hu et al., 2008; Li et al., 2022; Wortham et al., 2022); and (2) estimation of R02i using linear binary mixing models or a priori assumptions to obtain continuous chronologies. In cases where direct measurement is not possible, the isochron method (binary mixing) can serve as a first order alternative. However, in order for this technique to be effective, multiple sub-samples from the same lamina (or group of laminae) must exhibit varying ²³²Th/²³⁸U ratios and follow first-order binary linear mixing behaviour (Wenz et al., 2016; Ludwig and Titterton, 1994). Another approach is the stratigraphic constraint method, where R02i is estimated by ensuring that the corrected ages increase steadily with distance from the top (dft) of the stalagmite (Roy-Barman and Pons-Branchu, 2016; Hellstrom, 2006). While monitoring detrital activity ratios in ZAC and drip waters provides useful information about initial activity ratios, it offers little insight into whether and how these ratios change over time.

High-resolution stalagmite records from the Yucatán Peninsula (YP) have been analysed to explore hydroclimate variability and its intersection with Maya sociopolitical evolution (e.g., Kennett et al., 2012; Medina-Elizalde et al., 2010). However, in the northeastern YP, high-resolution records are few, with only one stalagmite record available, spanning 1037 BCE to 397 AD (Medina-Elizalde et al., 2016b). Critically, YP records often face dating challenges due to low uranium concentrations or high detrital contamination (e.g., Frappier et al., 2014; Webster et al., 2007; Akers et al., 2016; Akers et al., 2019; James et al., 2025; Medina-Elizalde et al., 2010; Kennett et al., 2022). These complexities make it difficult to reconstruct past climate and environmental changes with precision, obscuring the evaluation of their effects on Maya cultural evolution, particularly during the Terminal Classic Period



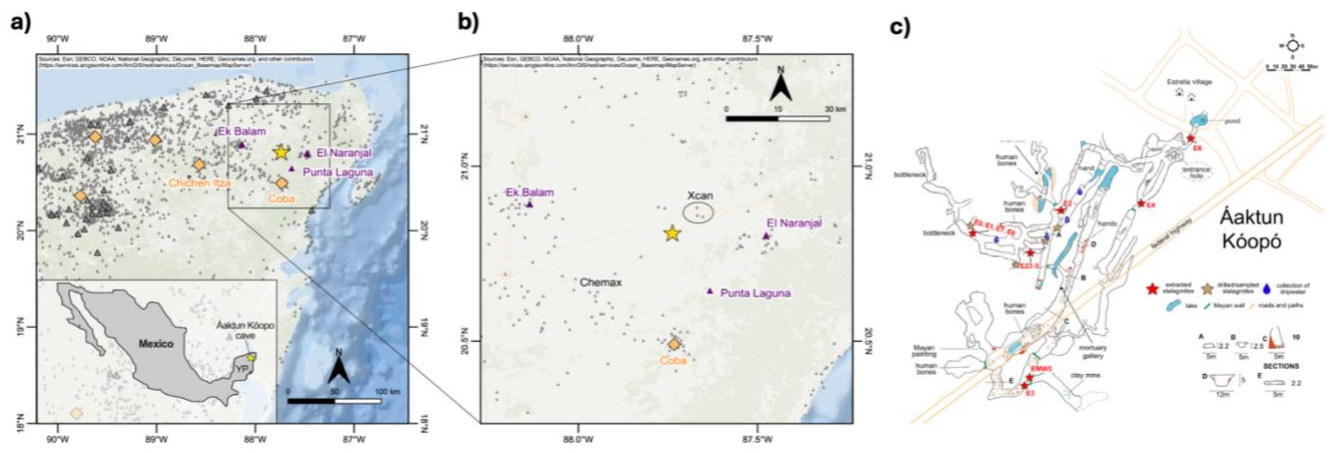
(TCP; ~800–1000 AD), a time of profound social and political upheaval marked by widespread population decline and the abandonment of many urban centres (e.g., Douglas et al., 2015).

95 This study focuses on constructing precise $^{230}\text{Th}/\text{U}$ chronologies for stalagmites from Áaktun Kóopo Cave, located in the northeastern YP. Through a detailed study of the speleothems' U and Th isotope compositions, their micro-facies and geochemistry, as well as their stable isotope compositions we establish multiple age-depth models that demonstrate active speleothem deposition over the past 2.7 kyr. These chronologies fill a notable gap in high-resolution paleoclimate records for the region and provide a foundation for future investigations into hydroclimatic and environmental changes, particularly during periods of profound Maya societal changes. Crucially, our study reveals highly variable initial ^{230}Th coprecipitation within the karst system that impacts, and in some layers inhibits, high-precision $^{230}\text{Th}/\text{U}$ age determination, thereby limiting the accuracy of speleothem chronologies. The chemical transport processes of Th isotopes in meteoric water, however, remain poorly understood.

2 Material and Methods

105 2.1 Study site

Áaktun Kóopo Cave is located in La Estrella, a small Maya community in the northeastern YP (Figure 1a). The cave lies approximately 30 km northeast of Chemax and 7 km southwest of Xcan, at $20^{\circ}48'26.7''\text{N}$, $87^{\circ}44'15.8''\text{W}$ (Figure 1b). Initial documentation of Áaktun Kóopo Cave by the AJAU cave explorers in 2007 recorded numerous archaeological remains. Subsequent exploration in 2010 extended the surveyed passages to a total length of 1900 m and a depth of 21 m (Thomas, 2011), and more recent mapping indicates over 2100 m of horizontal passage (Tec, 2021) (Figure 1c). There are at least nine distinct water bodies within the cave, and their water levels fluctuate seasonally between the rainy and dry seasons, which occasionally results in localized flooding in some parts of the cave (Tec, 2021). Cave sediments typically consist of red clay (kankab) that ranges from dry to muddy conditions. Archaeological evidence inside the cave includes Maya paintings, polychrome pottery, and skeletal remains of 23 individuals (juveniles and adults), dating to the Late Preclassic (–250 to 300 AD) and Early Classic (300–600 AD) periods (Gómez, 2020). The Maya also modified parts of the cave by constructing walls using limestone blocks, speleothems, and soil to create chambers (Tec, 2021). The presence of imported materials such as flint and obsidian (Gómez, 2020) suggests that members of the local elite performed mortuary and ritual practices in the cave. In addition to these archaeological features, Áaktun Kóopo Cave is decorated with numerous speleothem formations, including stalactites, stalagmites, flowstones, and draperies, making it an important site for both archaeological and paleoclimate research.



125 **Figure 1: a) Location of the Áaktun Kóopó Cave (yellow asterisk) in the northeastern Yucatán Peninsula, Mexico, relative to other**
Maya archaeological settlements in the area. b) Zoom-in showing the settlement density around Áaktun Kóopó Cave, with well-
known settlements such as Coba, Punta Laguna, El Naranjal, and Ek Balam, all within 20–40 km distance, and the closest settlement,
Xcan (encircled), less than 10 km to the northeast. Orange diamonds represent large settlements while large (small) triangles
represent intermediate (smallest) ones, based on Witschey and Brown (2010). c) Map of Áaktun Kóopó Cave with sample locations.
Red stars show locations of stalagmites that have been extracted from the cave, while brown stars represent locations where samples
were drilled or scraped from stalagmites. Blue symbols mark sites of drip water collection. Map was taken from Thomas (2011) and
 130 **modified after Gómez (2020) and Tec (2021).**

2.2 Sample material

During three cave visits in 2018, 2022, and 2023, samples for $^{230}\text{Th}/\text{U}$ dating were collected from 15 different speleothems inside Áaktun Kóopó Cave, including stalagmites, flowstones, and modern carbonate deposits. In addition to in-situ drill cores from various speleothems, ten stalagmites, ranging from 6.5 to 34 cm in length, were
 135 extracted completely for more detailed analysis (Figure S 1). For six of these stalagmites (E0, E1, E2, E7, E8, E23-3) their drip site was still actively dripping at the time of collection. Stalagmites E0, E1, E7, and E8 were all collected from a c. two square metre area in the northwestern part of the cave (Figure 1c). Interestingly, both E0 and E7 exhibited an L-shaped, or "double" formation (Figure S 1). This morphology occurs when a stalagmite falls over, and continued carbonate precipitation causes growth to proceed at a perpendicular angle to the original axis,
 140 resulting in the observed L-shape. Notably, E0 was not calcified to the ground but rather embedded in soft sediment, which may have contributed to its collapse. During the extraction, a third stalagmite (E0-A) was uncovered beneath 10 cm of sediment. Stalagmite E2 was collected from the central part of the cave, while stalagmite E4 was retrieved from the northeastern section, closer to the cave's entrance. Stalagmite E3 was collected from the southern portion, located in front of a large Maya wall, from which a small stalagmite (EMW5) detached and was collected as well.
 145 Furthermore, we collected three drip water samples (EDW-1, EDW-2 and EDW-3) from different parts of the cave in 2022 (Figure 1c) to evaluate the R02i in drip water. EDW-3 consists of an integrated water sample collected



from different drips (soda straws) with low drip rates within an area of about 1 m² within the chamber in the western part of the cave where most of the analysed stalagmites were extracted (Figure 1c). After drip water collection, the plastic bottles (125 ml) were immediately sealed with Parafilm for transportation and storage upon measurement.

150 From the floor below the drip site EDW-1, we collected a small sample of what appeared to be modern carbonate precipitates.

2.3 Mineralogical Characterization of Stalagmites

2.3.1 XRD Measurements

Slices of stalagmites from Áaktun Kóopo Cave revealed several changes in colour throughout their growth (Figure S 1), which may indicate changes in mineralogy or crystal fabrics. To investigate these variations and determine the mineralogical composition of the stalagmites (e.g., calcite vs. aragonite), nine samples were analysed from visually distinct sections of stalagmite E0-C for XRD analysis (Figure S 2a). Additionally, a sample was collected from the bottom portion of stalagmite E1, where the fan-like crystal texture and silky gloss suggested aragonite as the dominant polymorph (Figure S 1 and S 2). Each sample consisted of approximately 1 g of carbonate powder that was drilled using a Proxxon machine equipped with a diamond-coated stainless-steel drill bit. XRD measurements were performed at the Institute of Earth Sciences, Heidelberg University, using a Bruker D8 ADVANCE Eco diffractometer. The measurements were conducted with the following parameters: Cu K radiation source, 30 kV voltage, 33 mA current, Ni filter, SSD160 detector. Samples were analysed in rotating sample holders over an angular range of 2 θ from 5° to 70°, with increments of 0.019° and a counting time of 1 second per step. Peak positions and intensities were processed using Diffrac.Suite EVA software (Bruker).

165

2.3.2 Thin section inspection

Thin sections have been used to study the crystal fabrics in further detail, i.e. the individual expression of mineral phases, direction, non-carbonate contamination and/or signs of dissolution (e.g., Frisia et al., 2002; Perrin et al., 2014). Thin sections were prepared from stalagmites E0-B, E0-C, E4, E8, and the upper section of E1. These sections were analysed under a polarized transmitted-light microscope (KEYENCE VHX-6000) at the Institute of Earth Sciences, Heidelberg University.

170



2.4 Geochemistry

2.4.1 In-situ Strontium – Calcium analysis

Laser ablation ICP-MS analyses of selected stalagmites and for Sr/Ca ratios followed established protocols
175 (Warken et al., 2021; Jochum et al., 2012; Schorndorf, 2024) and were performed using a 193 nm ArF excimer
laser (NWR193UC by New Wave Research) coupled to an inductively coupled plasma quadrupole mass
spectrometer (Thermo Fisher iCAP-Q) at the Institute of Environmental Physics, Heidelberg University. Line scans
were conducted along the growth axis of the stalagmite slices using a rectangular spot size of $25 \times 100 \mu\text{m}$. The
repetition rate was set to 20 Hz, with scan speeds of $5 \mu\text{m s}^{-1}$ for stalagmites E1 and E8, and $10 \mu\text{m s}^{-1}$ for stalagmite
180 E23-3. To eliminate potential surface contamination, a pre-ablation step was performed along each scan path using
a circular spot size of $150 \mu\text{m}$ at a scan speed of $100 \mu\text{m s}^{-1}$ and a repetition rate of 10 Hz. Background counts were
measured with the laser in the off mode and subtracted from the raw data. Data processing involved an outlier
correction using a floating 1.5 interquartile range (IQR). To account for matrix effects, blank-corrected count rates
of ^{43}Ca and ^{88}Sr were normalized to the ^{44}Ca signal, which served as an internal standard for the total ablation
185 efficiency. External calibration was performed using silicate glass NIST SRM 612, with reference values provided
by Jochum et al. (2011). Drift corrections were applied through linear interpolation between two standard
measurements taken before and after each ablation path. The resulting Sr/Ca elemental ratios are presented as mass
concentration ratios.

2.4.2 Stable isotope analysis

190 For stalagmites E0-C, E1, and E23-3, approximately 50–90 μg of powdered samples was drilled using a Micromill
(2010A Sherline) equipped with a micro milling cutter (TiSiN) of 500 μm in diameter. Most samples were analyzed
for their stable isotope composition of oxygen ($\delta^{18}\text{O}$) and carbon ($\delta^{13}\text{C}$) at the Institute of Earth Sciences,
Heidelberg University, using a ThermoFinnigan MAT253Plus gas source mass spectrometer equipped with a
Thermo Fisher Scientific Kiel IV carbonate device. Quality control is based on the analysis of an in-house standard
195 (Solnhofen limestone, $\delta^{13}\text{C}_{\text{VPDB}} = +1.38 \pm 0.03\text{‰}$ and $\delta^{18}\text{O}_{\text{VPDB}} = -4.59 \pm 0.06\text{‰}$) calibrated to the reference
material IAEA-603 (calcite; $\delta^{13}\text{C}_{\text{VPDB}} = +2.46 \pm 0.01\text{‰}$ and $\delta^{18}\text{O}_{\text{VPDB}} = -2.37 \pm 0.04\text{‰}$). A part of the samples of
E0-C was analysed at Elementex Ltd., Cornwall, UK, using an isotope ratio mass spectrometer (IRMS) (Thermo
Scientific Delta V) coupled with a Gasbench II). Here, quality control is performed using a Carrara marble standard
($\delta^{13}\text{C} = 2.10\text{‰}$, $\delta^{18}\text{O} = -2.01\text{‰}$) and a second in-house calcite standard ($\delta^{13}\text{C} = 2.89\text{‰}$, $\delta^{18}\text{O} = -6.15\text{‰}$), calibrated
200 directly against NBS18 and NBS19.



External reproducibility at both labs is better than 0.04‰ for $\delta^{13}\text{C}_{\text{VPDB}}$ and 0.07‰ for $\delta^{18}\text{O}_{\text{VPDB}}$ at the 1σ confidence level, and all $\delta^{13}\text{C}$ and $\delta^{18}\text{O}$ values are reported relative to Vienna Pee Dee Belemnite (VPDB) standard.

2.5 Chronology

2.5.1 $^{230}\text{Th}/\text{U}$ Dating

205 A total of 157 subsamples from Áaktun Kóopo speleothems were analysed using high-precision $^{230}\text{Th}/\text{U}$ dating performed with a multi-collector inductively coupled plasma source mass spectrometer (MC-ICP-MS, Thermo Fisher Neptune plus) at the Institute of Environmental Physics, Heidelberg University. Prior to the analysis, the stalagmites were cut along their presumed growth axis into slices. From these slices, small sample plates weighing approximately 100 mg were cut perpendicular to their growth direction using a diamond wire saw. The preparation
210 involved sample leaching, dissolution, spiking, and wet column extraction chromatography using Eichrom UTEVA resin, following established protocols (Wefing et al., 2017; Matos et al., 2015; Douville et al., 2010). Isotope measurements were conducted using a semi-static multi-cup setting as described by Kerber et al. (2023). Mass spectrometry techniques and data treatment adhered to procedures detailed in Kerber et al. (2023); (2025). Data analysis was performed using a Python-based GUI application (Kerber et al., 2025). Ages were calculated using
215 the half-lives provided by Cheng et al. (2013), and uncertainties are reported at the 2σ level, excluding errors associated with half-life values.

2.5.2 Radiocarbon Dating

To constrain recent carbonate deposition, the tops of presumably modern speleothems were analysed using radiocarbon dating. Small calcite samples (10–20 mg) were cut from the tops of stalagmites E0-C, E1, and E8 using
220 a diamond wire saw at the Institute of Environmental Physics, Heidelberg University. To avoid contamination by ambient air, the samples were leached in 4% hydrochloric acid prior to hydrolysis and graphitization. A detailed description of the sample preparation routine is provided in Therre et al. (2021). The resulting graphite–iron compounds were measured using a 200 kV tandem mini carbon dating system (MICADAS) accelerator mass spectrometer (AMS) at the Curt-Engelhorn Center for Archaeometry in Mannheim, Germany (Kromer et al., 2013;
225 Synal et al., 2007). Details regarding long-term blank values and external standard reproducibility can be found in Beisel et al. (2025) and Therre et al. (2021).



2.5.3 Speleothem age-depth models

The age-depth models for selected stalagmites were constructed using a suite of established approaches: linear interpolation, linear regression, Bchron (Haslett and Parnell, 2008), Bacon (Blaauw and Christen, 2011; Blaauw et al., 2021), COPRA (Breitenbach et al., 2012), and StalAge (Scholz and Hoffmann, 2011). Model construction followed and extended the protocols of the Speleothem Isotopes Synthesis and Analysis (SISAL) working group (Roesch and Rehfeld, 2020), which is provided as a supplement to Comas-Bru et al. (2020); SISAL.AM. In case of identified hiatuses, the age-depth models were split at the depth of the growth interruption into separate sections. This approach improves model convergence and allows more methods to return successful chronologies, rather than including the hiatuses in the models. For each model, the median and the 2.5–97.5 % quantiles across the ensemble were extracted to define the central age estimate and its 95% uncertainty range at each depth. To derive the final chronology, all models that returned successful chronologies were included. At each depth, the composite chronology was calculated as the arithmetic mean of the selected models (equal weights):

$$\mu_{final}(d) = \frac{1}{N} \sum_{i=1}^N M_i(d)$$

where $M_i(d)$ is the age of model i at depth d , and N is the number of selected models. The corresponding 95 % uncertainty was derived by combining (i) the between-model spread (standard error of model ages) and (ii) the mean within-model uncertainty (average 95 % half-widths) in quadrature:

$$\sigma_{final,95} = \sqrt{\sigma_{between}^2 + \sigma_{within}^2}$$

Where geochemically defined annual cycles from Sr/Ca variations were identified, the resulting layer-count chronologies were treated as an independent constraint rather than being incorporated into the composite chronology. These were converted to absolute ages by anchoring the layer-count chronology either (i) to the year of stalagmite extraction, if continuous growth until collection can be assumed, or (ii) to the U-Th age with the smallest analytical uncertainty within the counted interval. For intervals in which seasonal variations were less pronounced or individual cycles were indistinct, a conservative uncertainty of ± 0.5 layers per 10 counted layers was assigned, reflecting the potential for missed or ambiguous cycles



3 Results

3.1 Speleothem Petrography

One XRD analysis of the bottom portion of stalagmite E1 verified the presence of aragonite, as initially suggested by its fan-like crystal texture and silky gloss (Figure S 2b). In contrast, all nine XRD measurements from different sections of stalagmite E0-C indicated the presence of pure calcite (Figure S 2a). Thin section analyses of stalagmites E0-B, E0-C, E1, E4 and E8 revealed only calcite phases. These primarily consisted of two fabrics: compact- and open-elongated calcite, with crystals exhibiting a length-to-width ratio greater than 6:1 (Frisia, 2015) (Figure S 3). Macroscopically, the compact elongated calcite phase appeared more translucent, while the open elongated fabric displayed a whitish appearance (Figure S 1). Growth interruptions (hiatuses) were macroscopically visible either as major flooding layers (Figure S 1) or as smaller detrital layers, typically near the tops of the stalagmites but occasionally occurring throughout their growth (Figure S 3). Under the microscope, these interruptions were characterized by clear rhombohedral crystal terminations and the presence of detrital minerals such as clay (Figure S 3). No evidence of aragonite-to-calcite recrystallization, such as preserved aragonite textures or "ghosts" of aragonite (Frisia et al., 2002; Perrin et al., 2014), was observed in any of the thin sections. Therefore, it is assumed that stalagmites E0-B, E0-C, E4, E8, and the upper portion of stalagmite E1 consist of primary calcite, predominantly in the form of compact or slightly open elongated fabrics.

3.2 Radiocarbon dating

A total of four ^{14}C measurements were performed on three different stalagmite tips (E0-C, E1, and E8), with one duplicate measurement taken from the E0-C sample (Table S 1). The measured ^{14}C activities ($a^{14}\text{C}_{\text{meas}}$) ranged from 97.54 ± 0.20 pmC to 94.95 ± 0.19 pmC. Assuming even only a minor contribution of "dead carbon" (<10%) to the carbonate in the stalagmite would result in $a^{14}\text{C}_{\text{meas}}$ values >100 pmC, which suggests modern growth (post-1950 AD) for the stalagmite tips.

3.3 $^{230}\text{Th}/\text{U}$ dating

$^{230}\text{Th}/\text{U}$ dating was performed on 157 speleothem sub-samples from Áaktun Kóopo Cave (Table S 2). The uranium content of the analysed speleothems spans from 106 to 2237 ng g $^{-1}$. Measured $\delta^{234}\text{U}$ values time independently average 14 ± 8 ‰ which is close to secular radioactive equilibrium with minimal variation, mirroring the low activity ratios of the drip (Table S 2) as well as local ground water (Schorndorf et al., 2023). ^{232}Th concentrations are generally low with values <0.1 ng g $^{-1}$, resulting in ($^{230}\text{Th}/^{232}\text{Th}$) activity ratios >300, indicating minor residual



initial Th influence. Overall, $^{230}\text{Th}/\text{U}$ dating suggests late Holocene speleothem growth for most studied stalagmites
280 from Àaktun Kóopo Cave, since most uncorrected ages cluster during the past c. 2.7 kyr (Table S 2). Notable
exceptions are stalagmites E6 or E23-1 where uncorrected ages suggest deposition between 333 ± 13 to 264.1 ± 5.7
kyr and 74.90 ± 0.20 to 16.735 ± 0.061 kyr, respectively.

However, several samples show elevated ^{232}Th (up to 26.5 ng g^{-1}), young ages, lower uranium concentrations, or a
combination of these factors. Consequently, measured $^{230}\text{Th}/\text{U}$ ages do not align stratigraphically, and many of the
285 inversions are not resolved when using a bulk Earth detrital ($^{230}\text{Th}/^{232}\text{Th}$) activity ratio of ~ 0.8 , typical for the upper
continental crust (Taylor and McLennan, 1985). Notably, the modern carbonate sample yielded an elevated
($^{230}\text{Th}/^{232}\text{Th}$) activity ratio of 6.57 ± 0.03 , while ($^{230}\text{Th}/^{232}\text{Th}$) activity ratios in three drip water samples from the
cave ranged from 1.659 ± 0.046 to 8.9 ± 1.0 (Table S 2), suggesting high levels of initial ^{230}Th in the system. Since
using the drip water or modern carbonate ($^{230}\text{Th}/^{232}\text{Th}$) activity ratio for age correction does not yield satisfying
290 results either, we infer that a more detailed inspection of the elevated initial ^{230}Th systematics is mandatory to
obtain reliable chronologies.

3.4 Sr/Ca ratios

For stalagmites E1, E8, and E23-3, LA-ICP-MS analyses revealed pronounced oscillations in Sr/Ca ratios from 0.1
to 0.66 mg/g, permitting identification of strong geochemical cycles (Figure S 4). These cycles serve as a potential
295 proxy for seasonal abundance changes of Sr relative to Ca and thus annual geochemical laminae (Warken et al.,
2018; Huang et al., 2001). The interval between two successive Sr/Ca minima is here interpreted as representing
one year. Annual cycles of strongly variable amplitude and distance were identified by plotting Sr/Ca ratios against
the dft and manually counting the distance between successive Sr/Ca minima. The minima appeared as the best
choice since those are sharper and more distinct than the broader maxima. This approach provides an independent
300 means to refine age-depth models derived from $^{230}\text{Th}/\text{U}$ dating (Smith et al., 2009) and may ultimately allow for
annual relative age precision of climate proxy data.

3.5 Stable isotope values

The stable isotopes of oxygen and carbon analyzed in stalagmites E0-C (Table S4), E1 (Table S5), and E23-3
(Table S6) yielded $\delta^{13}\text{C}$ values ranging between c. -7.9 ‰ and c. -12.4 ‰ , while the range of $\delta^{18}\text{O}$ values is between
305 c. -7.1 ‰ to c. -3.8 ‰ . Notably, the lowest and highest $\delta^{13}\text{C}$ and $\delta^{18}\text{O}$ values in all three stalagmites are very
similar, respectively.



4 Discussion

4.1 Determination of initial ($^{230}\text{Th}/^{232}\text{Th}$) ratios

$^{230}\text{Th}/\text{U}$ dating of Áaktun Kóopo Cave speleothems reveal a vast spread, including significant age inversions. Petrographic analyses exclude obvious dissolution effects which could have affected the quality of the ages. There is, however, strong evidence for elevated initial ^{230}Th in the Áaktun Kóopo cave system. Most age inversions are associated with elevated ^{232}Th concentrations and a relationship between ($^{230}\text{Th}/^{238}\text{U}$) and ($^{232}\text{Th}/^{238}\text{U}$) activity ratios, consistent with significant Th transport through the karst water, either associated to particles, colloids or chemical complexing agents (Ludwig, 2003). The resulting relationship follows a first order binary mixing, when activity ratios are plotted as Osmond type II isochrons (Figure 2a). Modern carbonate and drip water samples yielded variable R_{02i} of up to 8.9 ± 1.0 , but even with these elevated ratios applied to correct for detrital Th contamination, many speleothem age inversions persist. Consequently, higher R_{02i} are necessary in cases to meet the stratigraphic constraint of increasing ages from top to bottom (Hellstrom, 2006). To estimate the range of R_{02i} , different approaches are tested, including (i) isochrons and (ii) stratigraphic constraint. In addition, (iii) geochemical Sr/Ca cycles were used as annual layer counts to estimate relative age differences between Th/U ages and to independently test the other approaches (Domínguez-Villar et al., 2012; Nagra et al., 2017). Given the difficulty in accurately constraining R_{02i} , all samples with ratios <200 ($n=68$) were excluded from further discussion (Figure 2b), as they provide no meaningful chronological information due to the growing age uncertainty, when propagating the uncertainty of the correction model in the corrected ages. This criterion also applies to all samples within 7.5 mm of the stalagmite tops, as these were generally highly contaminated with limited ^{230}Th ingrowth.

4.1.1 Comparison of different approaches

Dense sampling in some stalagmites allows for linear two-endmember mixing regressions (Osmond type 1 isochrons) using ISOPLOT (Ludwig and Titterton, 1994; Ludwig, 2008; Vermeesch, 2018), similar to the approaches of Warken et al. (2020) or Stinnesbeck et al. (2020). The isochron approach produced five successful isochrons from three stalagmites (E0-C, E4, E8), which yielded R_{02i} ranging from 6.4 ± 2.4 to as large as 19 ± 10 (Figure S 5, Supplementary material S1.1). To apply stratigraphic constraints (e.g., Roy-Barman and Pons-Branchu, 2016; Hellstrom, 2006), we used samples with no detectable ^{232}Th as stratigraphic anchors, as their ages are unaffected by initial Th contamination and because those provide a steady growth pattern. In addition, we adopt the assumption that stalagmite tops with elevated ^{232}Th are younger than uncorrected ages below them, but older



than the year of collection. From Stalagmite E0-C, 34 of 51 samples could be placed in stratigraphic order using individual R02i ranging from 11.5 to 49 (Figure 4b). In contrast, for other stalagmites, such as E0-B or E1, only single ages can be corrected using a stratigraphically derived ratio. Lastly, we exploit distinct cyclic variations in Sr/Ca ratios from LA-ICP-MS measurements (Figure S 4) to estimate relative age differences between $^{230}\text{Th}/\text{U}$ measurements, thus allowing to correct the ages and estimate R02i (James et al., 2025). For example, in stalagmite E23-3, in total 331 ± 17 Sr/Ca minima are counted from 0 to 84 mm dft. Assuming the topmost layer to correspond to 2022 AD (the year of collection), the R02i is estimated to 26 ± 7 to align the $^{230}\text{Th}/\text{U}$ ages with the layer-counted age model presuming Sr/Ca seasonal cycles within uncertainties of both methods. In contrast, in the upper section of stalagmite E8 (8.5–26 mm dft), ages could only be corrected with individual R02i ranging from 7 to 35.5 to match the Sr/Ca-based age-depth model. Overall, to correct stalagmite ages with the different approaches, R02i ranging from 4 to 68 are found (Table S 2). Notably, only one sample from stalagmite E1 requires a ratio as high as 68, while most other samples need ratios between 30 and 50 or lower. R02i <20 are only found for three ages via stratigraphic constraint and for nine ages by isochrons. Therefore, samples without specific estimates, are corrected by using the mean ratio of 35.5 ± 32.5 to account for the full range of possible initial Th corrections (Table S 2).

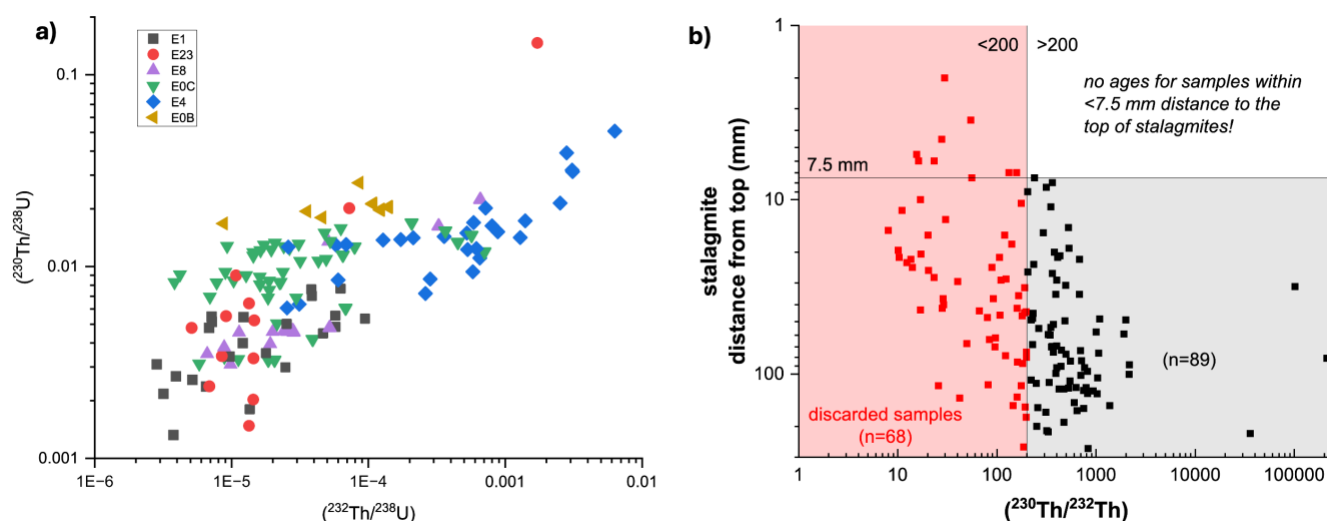


Figure 2. Activity ratios from various stalagmites in Áaktun Kóopo Cave. a) Relationship between $(^{230}\text{Th}/^{238}\text{U})$ and $(^{232}\text{Th}/^{238}\text{U})$ activity ratios. The observed linear trend indicates significant detrital contamination. Different symbols and colors correspond to individual stalagmites. Both axes are plotted on a logarithmic scale. b) $(^{230}\text{Th}/^{232}\text{Th})$ activity ratios. Samples with $(^{230}\text{Th}/^{232}\text{Th})$ activity ratios <200 (n=68, red squares) were excluded from age-depth models due to significant initial Th contamination. Remaining samples (n=89, black squares) were included in age-depth models and further analysis. No samples with $(^{230}\text{Th}/^{232}\text{Th})$ ratios >200 were observed within 7.5 mm of the stalagmite tops, due to the young age of these carbonates and limited ^{230}Th ingrowth.



4.1.2 Elevated and variable initial ($^{230}\text{Th}/^{232}\text{Th}$) ratios in Áaktun Kóopo cave

Overall, our analysis shows, that significantly elevated and strongly variable R02i (up to 68) are required to correct
360 stalagmite ages from Áaktun Kóopo Cave for initial Th contamination (Table S 2). These values greatly exceed the
commonly assumed upper continental crust ratio of ($^{230}\text{Th}/^{232}\text{Th}$) ~ 0.8 (Taylor and McLennan, 1985). However,
they align with findings from other tropical sites (e.g., the Caribbean and Southeast Asia) where similarly high
ratios have been reported (e.g., Beck et al., 2001; Richards and Dorale, 2003; Partin et al., 2007; Carolin et al.,
2013; Arienzo et al., 2015; Hoffmann et al., 2010; Moseley et al., 2015; Ridley et al., 2015; Stinnesbeck et al.,
365 2020; Vieten et al., 2024a; Vieten et al., 2024b; Steidle et al., 2021; Warken et al., 2021; James et al., 2025).
Furthermore, our measurements demonstrate that this pronounced variability is largely unsystematic, occurring not
only spatially across different stalagmites within the same cave, similar to findings in Larga Cave, Puerto Rico
(Vieten et al., 2024b; Warken et al., 2020; Kerber et al., 2025) , but also temporally within individual stalagmites.
The vast spread of R02i may be attributed to the varying contributions of multiple Th reservoirs within the karst
370 and epikarst environments (Li et al., 2022; Wortham et al., 2022; Huang et al., 2024). Rather than a single source,
Th can be transported as a complex mixture of detrital particles (e.g., clay minerals, aluminosilicates, iron
oxyhydroxides), colloidal phases, and organic complexes (Morton et al., 2001; Nascimento et al., 2019; Reiller et
al., 2002; Richards and Dorale, 2003). In tropical environments with relatively young reef limestones as host rock,
such as the YP, the rapid dissolution and varying mobilization of these different organic and inorganic fractions
375 lead to highly variable initial Th isotopic signatures. This dynamic reflects the observations from various aquatic
systems, where the ($^{230}\text{Th}/^{232}\text{Th}$) activity ratio has been shown to vary by orders of magnitude (Scott, 1968; Hubert
et al., 2006; Hirose et al., 2012; Töchterle et al., 2022; Moore and Sackett, 1964; Moore, 1981). Consequently,
highly elevated and time-variable R02i should be regarded as the rule rather than the exception in such settings,
fundamentally questioning the applicability of a static 'bulk earth' value for age corrections.

380 Because we do not find any systematic behaviour that would allow to predict R02i a priori, developing accurate
age models remains challenging, even assuming simple binary (linear) mixing. Initial Th corrections are
particularly critical for younger speleothems (less than a few thousand years old), as even small uncertainties in the
R02i can significantly influence age models. While monitoring ZAC and drip water provides a baseline for
estimating R02i (Wortham et al., 2022; Li et al., 2022), this approach often fails to capture long-term temporal
385 variability. In Áaktun Kóopo Cave, for example, the ($^{230}\text{Th}/^{232}\text{Th}$) activity ratio from supposedly modern carbonate
and drip-water samples remain far below the highest estimated ratios (up to 68) required to align stalagmite ages
with the sedimentary sequence. Therefore, to reduce the uncertainty of corrected ages in similar karst settings, it is



strongly recommended to employ a combination of independent validation methods. Integrating $^{230}\text{Th}/\text{U}$ dating with radiocarbon or other radiometric dating methods (Akers et al., 2019; Huang et al., 2024; Sengupta et al., 2025) or annual layer counting (e.g., Warken et al., 2025; Domínguez-Villar et al., 2012; James et al., 2025; Faraji et al., 2021; Nagra et al., 2017) provides a more robust framework to constrain these erratic detrital inputs and secure reliable chronologies.

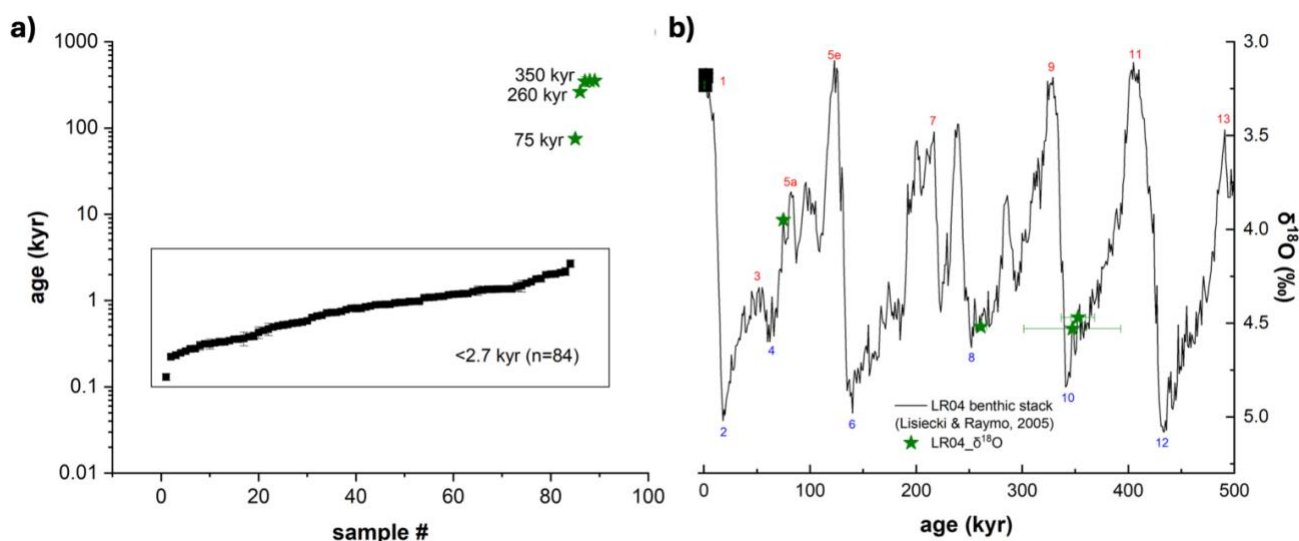


Figure 3 a) Distribution of speleothem samples according to their corrected ages on a logarithmic scale. Most samples are younger than 2.7 kyr, with some carbonate deposition at ~75 kyr, 260 kyr, and 350 kyr. (b) $^{230}\text{Th}/\text{U}$ ages plotted against the LR04 benthic $\delta^{18}\text{O}$ stack (Lisiecki and Raymo, 2005), highlighting deposition during earlier glacial and interglacial periods, with marine isotope stages shown in blue and red.

4.2 The Àaktun Kóopo Chronology

The finally corrected ages of speleothems from Àaktun Kóopo Cave range from as old as 353 ± 7 kyr to as young as 0.13 ± 0.015 kyr (Table S 2). Five older samples indicate speleothem growth during earlier glacial and interglacial periods, but most samples (84 out of 89) are younger than 3 kyr (Figure 3). Even though most $^{230}\text{Th}/\text{U}$ samples with low ($^{230}\text{Th}/^{232}\text{Th}$) activity ratios < 200 were rejected, radiocarbon measurements on speleothem tops (E1, E0-C, E8) as well as seasonal Sr/Ca chronologies (E1, E8, E23-3) suggest carbonate deposition within the last 130 years, likely continuing up to the present (Supplementary material S1.1). Overall, the stalagmites from Àaktun Kóopo Cave provide a robust basis for paleoclimatic and paleoenvironmental reconstructions over the late Holocene.



4.2.1 Late Holocene speleothem growth history

Figure 4 shows the individual age-depth models constructed for stalagmites E0-B, E0-C, E1, E4, E8, and E23-3, as described in detail in the Methods section and Supplementary material S1.1. Although some of the analysed stalagmites exhibit decade-long growth interruptions, their chronologies overlap and suggest continuous carbonate deposition in Àaktun Kóopo Cave over the last 2.7 kyr with mean growth rates of 200–300 $\mu\text{m a}^{-1}$ (Figure 5). While E0-B covers the oldest growth period (633 ± 161 BC to 403 ± 54 AD, Figure 4a), the growth of its “sibling” E0-C can be divided into three periods separated by hiatuses: (1) 538 ± 56 AD to 811 ± 52 AD; (2) 994 ± 29 AD to 1311 ± 15 AD; and (3) 1451 ± 22 AD to 1835 ± 53 AD (Figure 4b). The last millennium is also covered by several speleothems (Figure 5), with E1 growing from 1440 ± 39 AD to 1577 ± 42 AD and between 1635 ± 24 AD to 1926 ± 20 AD (Figure 4c). Stalagmite E4 grew from approximately 228 ± 88 AD to 1611 ± 118 AD, even though high initial Th contamination led to the rejection of 24 of 28 samples (Figure 4d). Similar challenges arose for the chronology of E8, where growth could be tightly constrained for the latest part (1605 ± 24 AD to 1733 ± 33 AD, Figure 4e). Lastly, the growth history of stalagmite E23-3 can be divided into two periods, with the older part covering 1070 ± 7 AD to 1347 ± 9 AD, and the upper part spanning 1441 ± 5 AD to the year of collection in 2022 AD (Figure 4f).

Figure 5 compares the late Holocene Àaktun Kóopo Cave growth history with periods covered by other published stalagmite records from the northern YP. Notably, while most records are from the northwestern YP (Kennett et al., 2022; Medina-Elizalde et al., 2010; James et al., 2025; Frappier et al., 2014; Medina-Elizalde et al., 2016a; James, 2024) there is a marked absence of stalagmite proxy records from the northeastern YP for the last 1600 years, with only one record covering an earlier period between 1037 BC and 397 AD (Medina-Elizalde et al., 2016b). Given the known regional heterogeneity in past hydroclimate reconstructions and projected trends, the Àaktun Kóopo Cave record thus fills an important gap in the region (Douglas et al., 2016; Obrist-Farner et al., 2023; Steinman et al., 2022).

430

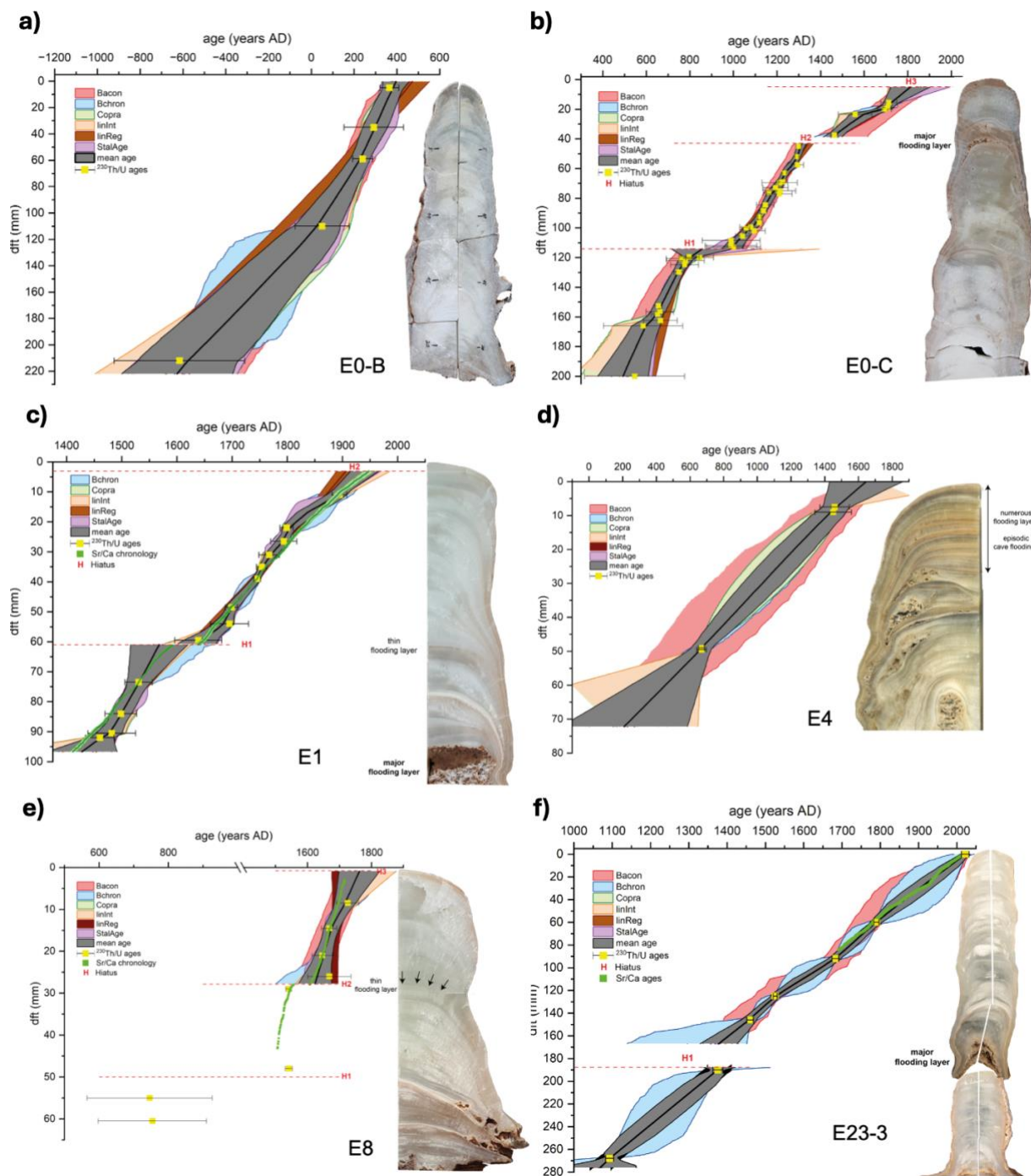
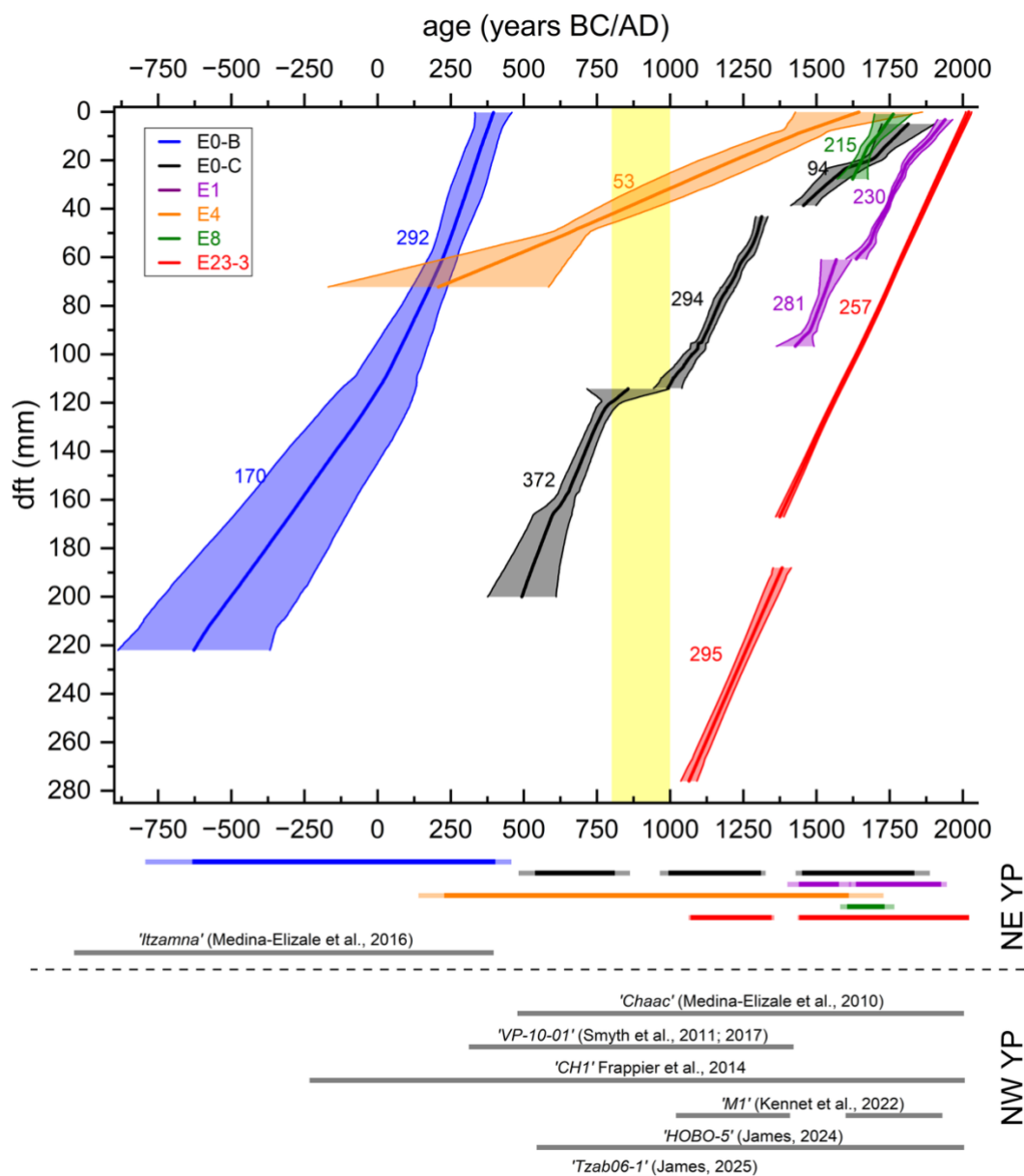


Figure 4 Age-depth models for Aaktun Koopo Cave stalagmites E0-B (a), E0-C (b), E1 (c), E4 (d), E8 (e) and E23-3 (f), generated using Bacon, Bchron, Copra, linInt, linReg, and StalAge, respectively. The final composite age-depth model is shown in black with its corresponding 95 % uncertainty band in grey, representing the arithmetic mean of the six model chronologies (equal weights). The $^{230}\text{Th}/\text{U}$ ages used in the models are indicated along with identified growth hiatuses and major flooding layers (E0-C, E1, E4, E8, E23-3). A scan of each stalagmite is shown on the right of each plot.

435



440 Figure 5 Mean age-depth models for stalagmites E0-B, E0-C, E1, E4, E8, and E23-3 from Áaaktun Kóopo Cave. Numbers indicate
 the average growth rates (in $\mu\text{m a}^{-1}$) during different growth periods. The coloured horizontal bars at the bottom illustrate the
 overlapping growth periods of the stalagmites over the last 2.7 kyr, highlighting intervals of simultaneous growth across multiple
 stalagmites. Lighter shades within the bars reflect the associated age uncertainties. Grey bars indicate periods covered by other
 445 published stalagmite records from the northern Yucatán Peninsula (YP). Notably, while most records are from the northwestern
 YP (Kennett et al., 2022; Medina-Elizalde et al., 2010; James et al., 2025; Frappier et al., 2014; Medina-Elizalde et al., 2016a; James,
 2024), there is presently a marked absence of stalagmite proxy records from the northeastern YP for the last 1600 years, with only
 one record covering an earlier period between 1037 BC and 397 AD (Medina-Elizalde et al., 2016b).



4.2.2 Origin of flooding layers and other growth interruptions

While precise $^{230}\text{Th}/\text{U}$ dating establishes the absolute chronological framework for these stalagmites, the numerous growth interruptions (hiatuses) observed throughout their growth histories provide an additional, independent
450 means to cross-validate these highly corrected age models. Detectable either as macroscopic millimeter- to centimeter-thick mud layers or via microscopic thin-section analysis, these hiatuses indicate discrete environmental events that simultaneously affected multiple stalagmites within the cave (Figure 4).

One prominent flooding layer (~ 1 cm thick) appears in E0-C, E1, and E23-3, likely representing a single event around 1400 AD. By comparing the $^{230}\text{Th}/\text{U}$ dates across the stalagmites, the timing can be constrained between
455 ~ 1350 AD and ~ 1430 AD. The latest confirmed carbonate precipitation prior to the event is recorded by stalagmite E23-3, which yielded a $^{230}\text{Th}/\text{U}$ age of 1347 ± 9 AD. Following the flood, stalagmite E1's growth resumed directly upon the detrital substrate at 1428 ± 40 AD. The sediment sequence of Sullivan et al. (2025) from Cenote Muyil c. 80 km south of Àaktun Kóopo cave recorded a period of intense hurricane activity between 1285 to 1420 AD in the area, which suggests that a major storm event may have caused the flooding of the cave during that time. Indeed,
460 historical records report a major hurricane ("hurricane of the four winds") that impacted the area in 1464 AD (Sullivan et al., 2025; Masson and Lope, 2014), which is however not fully consistent with our date, suggesting another extreme event caused the mud layer in Àaktun Kóopo Cave. Thinner layers (0.5–1 mm) in stalagmites E1 and E8 correspond to a shorter interruption that may have lasted only months to years. The timing can be precisely dated to 1624 ± 24 AD within the continuous age models of stalagmite E8, perfectly aligning with a brief hiatus
465 observed in E1 between ~ 1590 AD and ~ 1630 AD. In addition to detecting and dating single extreme events that may have impacted the environment and the people living in the area, such markers could serve as key stratigraphic tie-points, analogous to ash layers in marine sediments or ice cores, for anchoring proxy records and refining chronologies (Warken et al., 2025). Fine laminations (alternating carbonate and mud/clay) of stalagmite E4 even suggest recurrent flooding in the part of the cave near the entrance. While the current efforts limit a more precise
470 dating of the individual layers, future studies could deliver a more detailed history of local flooding (Frappier et al., 2014; Denniston and Luetscher, 2017; Gonzalez-Lemos et al., 2015).

Although many hiatuses coincide with clear flooding layers, other interruptions could reflect periods of reduced effective moisture due to reduced precipitation and/or enhanced evapotranspiration, or other processes. For example, the special morphology of Àaktun Kóopo Cave (Figure 1c) makes it conceivable, that a sufficiently high-
475 water table sealed cave ventilation in some sections of the cave, leading to elevated cave CO_2 . Because Àaktun Kóopo Cave was visited and modified by the Maya, at least during the Late Preclassic (-250 to 300 AD) and Early



Classic (300–600 AD) periods (Gómez, 2020), human influences on speleothem development can also not be ruled out. Deforestation and agricultural practices above the cave, for example, may have altered soil cover and infiltration pathways, thereby influenced recharge and ultimately affected speleothem formation. Likewise, cave use and ritual activities might have modified the cave's microclimate (e.g., CO₂ concentration, humidity, temperature) in ways that impacted speleothem formation, although such influences remain speculative. Disentangling natural hydrological variability from potential anthropogenic influences on speleothem formation remains a challenging task and requires a comprehensive multi-proxy approach that explores all aspects of speleothem formation, aimed at separating climatic from human-induced signals.

4.3 Age model uncertainties and algorithm comparison

4.3.1 Evaluation of the chronologies

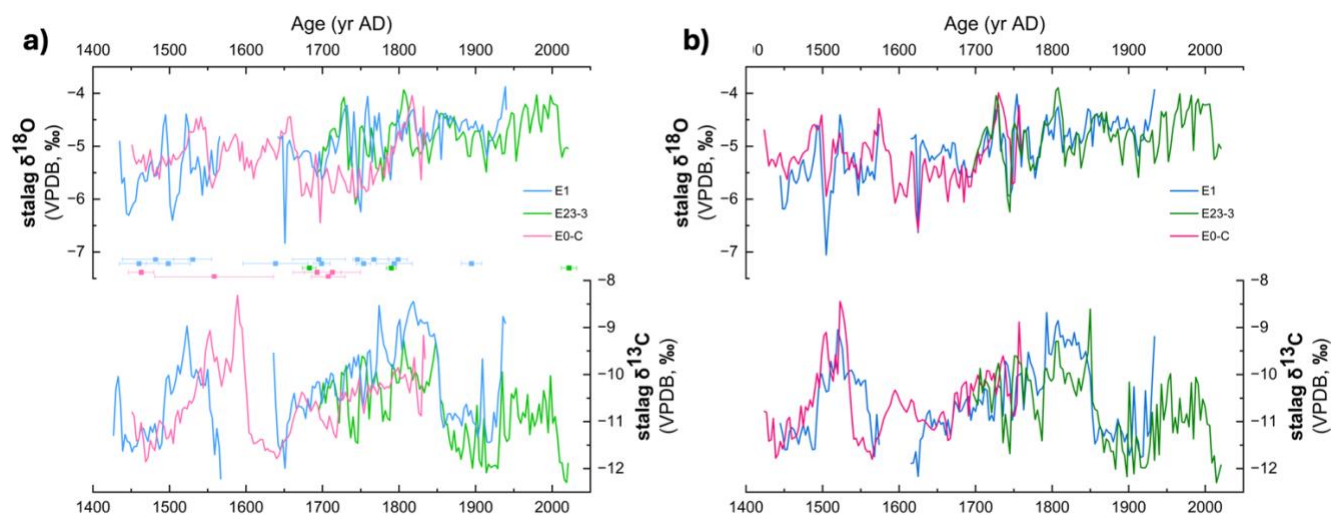
Evaluating the diverse performance of the applied age-depth modelling algorithms reinforces the necessity of our ensemble approach. Consistent with Comas-Bru et al. (2020), no single algorithm universally outperformed the others across all speleothems, as the underlying statistical assumptions of each model respond differently to variations in growth rates and dating resolution. This methodological variability becomes especially evident when comparing the models against independent layer-counting chronologies: while the Bacon model closely matched the visual layer counts for stalagmite E23-3, Bchron and linear interpolation provided the tightest fits for different sections of E8. Furthermore, the individual algorithms diverged significantly in their chronological treatment of extreme events, such as the major flooding layers and resulting hiatuses. The chosen algorithm significantly affects not only the estimated duration of an event, but also its absolute timing. For instance, the first hiatus in stalagmite E0-C (at 40 mm depth) has an estimated duration ranging from 96 (+58/–55) years (linear regression) to 174 (+85/–88) years (Bacon). Consequently, the absolute timing of the growth interruption shifts across models: Bchron dates the onset of the hiatus to 1302 (+25/–4) AD, whereas linear regression places it almost four decades later at 1341 (+26/–25) AD. Constructing a composite "mean" age model is therefore justified, relying on any single algorithm risks either artificially over-smoothing or over-estimating the timing and duration of discrete environmental events.

4.3.2 Validation of age models via stable isotope comparison

To further assess the robustness of our age models, we compared the independent stable oxygen ($\delta^{18}\text{O}$) and carbon ($\delta^{13}\text{C}$) isotope records of stalagmites E0-C, E1, and E23-3 for their overlapping growth periods. The chronology of stalagmite E23-3 is considered the most reliable anchor for the last 400 years. It is constrained by continuous counting of seasonal Sr/Ca cycles and anchored to the year of extraction (2022 AD), resulting in a cumulative



counting error of ± 17 year at 1691 AD. When plotting the stable isotope time series using the individually established $^{230}\text{Th}/\text{U}$ age-depth models, the records already show an apparent coherence in both $\delta^{18}\text{O}$ and $\delta^{13}\text{C}$ values over the past 600 years (Figure 6a). Despite being fed by different drip sites within the same cave chamber, the stalagmites capture nearly identical multi-decadal to centennial-scale geochemical patterns. This coherence suggests that the individual proxy records are driven by a common external forcing, such as regional hydroclimate variability affecting cave recharge and prior calcite precipitation (PCP), rather than localized kinetic or drip-specific effects (Skiba and Fohlmeister, 2023; Baker et al., 2019; Treble et al., 2022). However, the individual chronologies appear to be shifted relative to each other, reflected in the weak or insignificant correlations between the stable isotope records. For example, the largest significant coefficient of 0.2 ($p < 0.01$) occurs for the $\delta^{18}\text{O}$ records of E23-3 and E1. To precisely align the time series, a wiggle-matching procedure was performed using QAnalySeries software (Kotov and Pálike, 2018; Pálike), similar to the approach of Huang et al. (2024). The upper section of the E1 $\delta^{18}\text{O}$ record (3–61 mm dft) was tuned to the E23-3 reference record using 10 tie points, while the upper section of E0-C (5–38.6 mm dft) was subsequently matched to E1 using 11 tie points. As a result, the maximum shift of E1 with respect to E23-3 is c. 20 years directly after the thin flooding layer around 1620 AD, while the other sections are only corrected by < 7 years. The chronology of E0-C requires larger shifts by around 25–70 years with respect to E23-3. Overall, the resulting adjustments required to align these independent records fall entirely within the calculated 95% uncertainty ranges of their respective $^{230}\text{Th}/\text{U}$ age-depth models (Figure 6b).



525 **Figure 6. Stable oxygen ($\delta^{18}\text{O}$) and carbon ($\delta^{13}\text{C}$) records of speleothems E1, E23-3 and E0-C for the period from 1400 to 2022 AD binned to three-year averages, respectively. In panel a), the records are plotted on their original age scale. In addition, the respective $^{230}\text{Th}/\text{U}$ ages are shown to indicate the uncertainty in the respective chronologies. Panel b) shows the $\delta^{18}\text{O}$ and $\delta^{13}\text{C}$ records on the composite timescales, demonstrating a remarkable agreement. Note that the overlap between E23-3 and E0-C is too short to calculate meaningful correlation coefficients.**



After the synchronization, the $\delta^{18}\text{O}$ ($\delta^{13}\text{C}$) record of E1 exhibits a correlation of 0.62 (0.61) with E23-3 and 0.42
530 (0.51) with E0-C ($p < 0.01$, respectively), demonstrating a striking coherence between the stalagmite records. The
successful replication of stable isotope patterns across three distinct stalagmites and the tuning required to
synchronize them strongly validate our geochronological approach. It demonstrates that the strategies used to
correct for elevated and highly variable initial ^{230}Th contamination, specifically the integration of $^{230}\text{Th}/\text{U}$ dating
with seasonal trace-element layer counting and stratigraphic constraints, yield robust and accurate chronologies
535 suitable for high-resolution paleoclimate reconstruction on the YP.

5 Conclusions

Reconstructing reliable paleoclimate records from speleothems requires highly precise chronologies, which are
frequently compromised by variations of initial Th contamination through time in tropical karst environments. In
this study, we generated robust age-depth models for multiple late Holocene stalagmites from Áaktun Koopo Cave,
540 Yucatán, spanning the past 2.7 kyr. $^{230}\text{Th}/\text{U}$ dating revealed significant and highly variable initial Th contamination,
with initial ($^{230}\text{Th}/^{232}\text{Th}$) activity ratios ranging unpredictably between 4 and 68. These values vastly exceed
standard bulk earth corrections and demonstrate substantial spatial and temporal variability within the cave system.
This indicates that static initial Th corrections are insufficient in such settings, and modern drip-water or ZAC
monitoring may not capture the full range of initial ^{230}Th variability. To resolve chronological inversions, we
545 successfully employed a multi-method approach, combining isochron methods, stratigraphic constraints, and
relative seasonal layer counting (Sr/Ca). Our analysis highlights that different age-depth algorithms (e.g., Bacon,
Bchron, copRa, StalAge, Linear Regression) may yield different results, particularly when handling growth
discontinuities. This can affect both the estimated duration and the absolute timing of hiatus or other events; thus,
the integration of multiple constraints can yield more reliable chronologies. Ultimately, this comprehensive
550 chronological approach tackles the complexities of initial Th in Áaktun Kóopo Cave on the YP, providing a robust
foundational framework for future high-resolution proxy reconstructions of hydroclimate and environmental
change throughout the timeline of Maya cultural evolution. The resulting stable isotope climate proxy records show
outstanding coherence for the past 600 years.

6 Data availability

555 All data is available in the supplementary material.



7 Supplement link

The link to the supplement will be included by Copernicus, if applicable.

8 Author contributions

560 NS: Conceptualization, Formal analysis, Investigation, Validation, Visualization, Writing (original draft preparation), Writing (review and editing)

SW: Conceptualization, Formal analysis, Funding acquisition, Investigation, Supervision, Visualization, Writing (review and editing)

RE: Data curation, Formal analysis, Methodology

ASM: Investigation, Formal analysis, Data curation

565 JAO, FTP, CE, MJG: Resources

FK: Methodology, Resources, Data curation

DH: Formal analysis, Funding acquisition, Data curation

WS: Funding acquisition, Resources, Supervision

570 NF: Conceptualization, Funding acquisition, Investigation, Methodology, Resources, Supervision, Writing (review and editing)

9 Competing interests

A coauthor (Norbert Frank) is editor of Geochronology.

10 Disclaimer

Will be added by Copernicus.

575 11 Acknowledgements

We thank Julia Becker for helping with sample collection, and Antonia Wantzen and Alexander Slawik for supporting the sample preparation. We acknowledge support for stable isotope analysis by Stefan Rheinberger, Bernd Knape, Markus Greule, Alexa Fischer and Johannes Thommes. Steffen Therre and Ronny Friedrich are thanked for their help with ¹⁴C sample preparation and analysis, and Ilse Glass for XRD analysis.



580 Lastly, we dedicate this work to René Eichstädter, who passed away in 2025 after a long and very serious illness. René supported our team every day for more than 12 years with great enthusiasm and knowledge. His expertise in the mass spectrometry laboratory was invaluable, and he was a fantastic colleague, especially when we were doing field work. His commitment to his work was always very important to him and he would have loved to come back. We wish him a peaceful journey.

585 12 Financial support

This research has been supported by the Deutsche Forschungsgemeinschaft (grant nos. 247825108, 256561558, 497323584, and 512385350).

13 Review statement

The review statement will be added by Copernicus Publications listing the handling editor as well as all contributing
590 referees according to their status anonymous or identified.

14 References

- Akers, P. D., Brook, G. A., Railsback, L. B., Liang, F. Y., Iannone, G., Webster, J. W., Reeder, P. P., Cheng, H., and Edwards, R. L.: An extended and higher-resolution record of climate and land use from stalagmite MC01 from Macal Chasm, Belize, revealing connections between major dry events, overall climate variability, and Maya sociopolitical changes, *Palaeogeography Palaeoclimatology Palaeoecology*, 459, 268-288, 10.1016/j.palaeo.2016.07.007, 2016.
- 595 Akers, P. D., Brook, G. A., Railsback, L. B., Cherkinsky, A., Liang, F., Ebert, C. E., Hoggarth, J. A., Awe, J. J., Cheng, H., and Edwards, R. L.: Integrating U-Th, 14C, and 210Pb methods to produce a chronologically reliable isotope record for the Belize River Valley Maya from a low-uranium stalagmite, *The Holocene*, 29, 1234-1248, 10.1177/0959683619838047, 2019.
- Arienzo, M. M., Swart, P. K., Pourmand, A., Broad, K., Clement, A. C., Murphy, L. N., Vonhof, H. B., and Kakuk, B.: Bahamian speleothem reveals temperature decrease associated with Heinrich stadials, *Earth and Planetary Science Letters*, 430, 377-386, 10.1016/j.epsl.2015.08.035, 2015.
- 600 Baker, A., Hartmann, A., Duan, W., Hankin, S., Comas-Bru, L., Cuthbert, M. O., Treble, P. C., Banner, J., Genty, D., and Baldini, L. M.: Global analysis reveals climatic controls on the oxygen isotope composition of cave drip water, *Nature Communications*, 10, 2984, 2019.
- 605 Beck, J. W., Richards, D. A., Edwards, R. L., Silverman, B. W., Smart, P. L., Donahue, D. J., Hererra-Osterheld, S., Burr, G. S., Calsoyas, L., Jull, A. J., and Biddulph, D.: Extremely large variations of atmospheric 14C concentration during the last glacial period, *Science*, 292, 2453-2458, 10.1126/science.1056649, 2001.



Beisel, E., Therre, S., Wienberg, C., Friedrich, R., and Frank, N.: Status report of the Heidelberg Radiocarbon Laboratory: Precision and application in Mauritanian cold-water corals over the last 30,000 years, *Radiocarbon*, 67, 450-460, 2025.

610 Blaauw, M. and Christen, J. A.: Flexible paleoclimate age-depth models using an autoregressive gamma process, 2011.

Blaauw, M., Christen, J. A., Lopez, M. A. A., Vazquez, J. E., Belding, T., Theiler, J., Gough, B., Karney, C., Repp, L., and Blaauw, M. M.: Package ‘rbacon’, R package documentation, 2021.

Breitenbach, S. F., Rehfeld, K., Goswami, B., Baldini, J., Ridley, H., Kennett, D., Prufer, K., Aquino, V., Asmerom, Y., and Polyak, V.: Constructing proxy records from age models (COPRA), *Climate of the Past*, 8, 1765-1779, 2012.

615 Carolin, S. A., Cobb, K. M., Adkins, J. F., Clark, B., Conroy, J. L., Lejau, S., Malang, J., and Tuen, A. A.: Varied response of western Pacific hydrology to climate forcings over the last glacial period, *Science*, 340, 1564-1566, 2013.

Cheng, H., Edwards, R. L., Shen, C.-C., Polyak, V. J., Asmerom, Y., Woodhead, J., Hellstrom, J., Wang, Y., Kong, X., Spötl, C., and others: Improvements in ^{230}Th dating, ^{230}Th and ^{234}U half-life values, and U–Th isotopic measurements by multi-collector inductively coupled plasma mass spectrometry, *Earth and Planetary Science Letters*, 371, 82-91, 2013.

620 Comas-Bru, L., Rehfeld, K., Roesch, C., Amirnezhad-Mozhdehi, S., Harrison, S. P., Atsawawaranunt, K., Ahmad, S. M., Ait Brahim, Y., Baker, A., Bosomworth, M., Breitenbach, S. F. M., Burstyn, Y., Columbu, A., Deininger, M., Demény, A., Dixon, B., Fohlmeister, J., Hatvani, I. G., Hu, J., Kaushal, N., Kern, Z., Labuhn, I., Lechleitner, F. A., Lorrey, A., Martrat, B., Novello, V. F., Oster, J., Pérez-Mejías, C., Scholz, D., Scroton, N., Sinha, N., Ward, B. M., Warken, S., and Zhang, H.: SISALv2: A comprehensive speleothem isotope database with multiple age-depth models, *Earth Syst. Sci. Data Discuss.*, 2020, 1-47,
625 10.5194/essd-2020-39, 2020.

Denniston, R. F. and Luetscher, M.: Speleothems as high-resolution paleoflood archives, *Quaternary Science Reviews*, 170, 1-13, 2017.

Domínguez-Villar, D., Baker, A., Fairchild, I. J., and Edwards, R. L.: A method to anchor floating chronologies in annually laminated speleothems with U–Th dates, *Quaternary Geochronology*, 14, 57-66, 10.1016/j.quageo.2012.04.019, 2012.

630 Douglas, P. M., Pagani, M., Canuto, M. A., Brenner, M., Hodell, D. A., Eglinton, T. I., and Curtis, J. H.: Drought, agricultural adaptation, and sociopolitical collapse in the Maya Lowlands, *Proc Natl Acad Sci U S A*, 112, 5607-5612, 10.1073/pnas.1419133112, 2015.

Douglas, P. M. J., Demarest, A. A., Brenner, M., and Canuto, M. A.: Impacts of Climate Change on the Collapse of Lowland Maya Civilization, *Annual Review of Earth and Planetary Sciences*, Vol 44, 44, 613-645, 10.1146/annurev-earth-060115-012512, 2016.
635

Douville, E., Sallé, E., Frank, N., Eisele, M., Pons-Branchu, E., and Ayrault, S.: Rapid and accurate U–Th dating of ancient carbonates using inductively coupled plasma-quadrupole mass spectrometry, *Chemical Geology*, 272, 1-11, 10.1016/j.chemgeo.2010.01.007, 2010.

640 Faraji, M., Frisia, S., Hua, Q., Borsato, A., and Markowska, M.: Accurate chronological construction for two young stalagmites from the tropical South Pacific, *Quaternary Geochronology*, 74, 101415, 2023.

Faraji, M., Borsato, A., Frisia, S., Hellstrom, J. C., Lorrey, A., Hartland, A., Greig, A., and Matthey, D. P.: Accurate dating of stalagmites from low seasonal contrast tropical Pacific climate using Sr 2D maps, fabrics and annual hydrological cycles, *Scientific Reports*, 11, 2178, 10.1038/s41598-021-81941-x, 2021.



- 645 Fensterer, C., Scholz, D., Hoffmann, D., Mangini, A., and Pajón, J. M.: $^{230}\text{Th}/\text{U}$ -dating of a late Holocene low uranium speleothem from Cuba, IOP Conference Series: Earth and Environmental Science, 9, 012015, [10.1088/1755-1315/9/1/012015](https://doi.org/10.1088/1755-1315/9/1/012015), 2010.
- Frank, N., Turpin, L., Cabioch, G., Blamart, D., Tressens-Fedou, M., Colin, C., and Jean-Baptiste, P.: Open system U-series ages of corals from a subsiding reef in New Caledonia: Implications for sea level changes, and subsidence rate, *Earth and Planetary Science Letters*, 249, 274-289, [10.1016/j.epsl.2006.07.029](https://doi.org/10.1016/j.epsl.2006.07.029), 2006.
- 650 Frappier, A. B., Pyburn, J., Pinkey-Drobnis, A. D., Wang, X., Corbett, D. R., and Dahlin, B. H.: Two millennia of tropical cyclone-induced mud layers in a northern Yucatán stalagmite: Multiple overlapping climatic hazards during the Maya Terminal Classic “megadroughts”, *Geophysical Research Letters*, 41, 5148-5157, 2014.
- Frisia, S.: Microstratigraphic logging of calcite fabrics in speleothems as tool for palaeoclimate studies, *International Journal of Speleology*, 44, 1-1, 2015.
- 655 Frisia, S., Borsato, A., Fairchild, I. J., McDermott, F., and Selmo, E. M.: Aragonite-calcite relationships in speleothems (Grotte de Clamouse, France): Environment, fabrics, and carbonate geochemistry, *Journal of Sedimentary Research*, 72, 687-699, 2002.
- Gómez, M. J.: *Práctica Mortuoria Maya Prehispánica En Una Cueva En El Oriente De Yucatán: Áaktun Kóopo*, Master, Escuela Nacional de Antropología e Historia (ENAH), Ciudad de México, 2020.
- 660 Gonzalez-Lemos, S., Müller, W., Pisonero, J., Cheng, H., Edwards, R. L., and Stoll, H. M.: Holocene flood frequency reconstruction from speleothems in northern Spain, *Quaternary Science Reviews*, 127, 129-140, 2015.
- Haslett, J. and Parnell, A.: A simple monotone process with application to radiocarbon-dated depth chronologies, *Journal of the Royal Statistical Society: Series C (Applied Statistics)*, 57, 399-418, 2008.
- 665 Hellstrom, J.: U–Th dating of speleothems with high initial ^{230}Th using stratigraphical constraint, *Quaternary Geochronology*, 1, 289-295, [10.1016/j.quageo.2007.01.004](https://doi.org/10.1016/j.quageo.2007.01.004), 2006.
- Hirose, K., Kikawada, Y., and Igarashi, Y.: Temporal variation and provenance of thorium deposition observed at Tsukuba, Japan, *Journal of environmental radioactivity*, 108, 24-28, 2012.
- 670 Hoffmann, D. L., Beck, J. W., Richards, D. A., Smart, P. L., Singarayer, J. S., Ketchmark, T., and Hawkesworth, C. J.: Towards radiocarbon calibration beyond 28ka using speleothems from the Bahamas, *Earth and Planetary Science Letters*, 289, 1-10, [10.1016/j.epsl.2009.10.004](https://doi.org/10.1016/j.epsl.2009.10.004), 2010.
- Hu, C., Henderson, G. M., Huang, J., Xie, S., Sun, Y., and Johnson, K. R.: Quantification of Holocene Asian monsoon rainfall from spatially separated cave records, *Earth and Planetary Science Letters*, 266, 221-232, 2008.
- 675 Huang, S., Cai, Y., Cheng, H., Xue, G., Cheng, X., He, M., Li, R., Ma, L., Wei, Y., Lu, Y., Yang, L., and Edwards, R. L.: An integrated study of constraining the initial ^{230}Th of a stalagmite and its implications, *Quaternary Geochronology*, 80, 101497, <https://doi.org/10.1016/j.quageo.2024.101497>, 2024.
- Huang, Y., Fairchild, I. J., Borsato, A., Frisia, S., Cassidy, N. J., McDermott, F., and Hawkesworth, C. J.: Seasonal variations in Sr, Mg and P in modern speleothems (Grotta di Ernesto, Italy), *Chemical Geology*, 175, 429-448, 2001.



- 680 Hubert, A., Bourdon, B., Pili, E., and Meynadier, L.: Transport of radionuclides in an unconfined chalk aquifer inferred from U-series disequilibria, *Geochimica et Cosmochimica Acta*, 70, 5437-5454, 2006.
- Ivanovich, M. and Harmon, R.: Uranium series disequilibrium. Applications to environmental problems. Clarendon, 1992.
- James, D.: Speleothem Palaeoclimatology in the Maya Lowlands of Northwestern Yucatán, Mexico, 2024.
- 685 James, D. H., Carolin, S. A., Breitenbach, S. F., Hoggarth, J. A., Lases-Hernández, F., Endsley, E. A., Curtis, J. H., Gallup, C. D., Milbrath, S., and Nicolson, J.: Classic Maya response to multiyear seasonal droughts in Northwest Yucatán, Mexico, *Science advances*, 11, eadw7661, 2025.
- Jochum, K. P., Scholz, D., Stoll, B., Weis, U., Wilson, S. A., Yang, Q., Schwalb, A., Börner, N., Jacob, D. E., and Andreae, M. O.: Accurate trace element analysis of speleothems and biogenic calcium carbonates by LA-ICP-MS, *Chemical Geology*, 318-319, 31-44, 10.1016/j.chemgeo.2012.05.009, 2012.
- 690 Jochum, K. P., Weis, U., Stoll, B., Kuzmin, D., Yang, Q., Raczek, I., Jacob, D. E., Stracke, A., Birbaum, K., Frick, D. A., Günther, D., and Enzweiler, J.: Determination of Reference Values for NIST SRM 610-617 Glasses Following ISO Guidelines, *Geostandards and Geoanalytical Research*, 35, 397-429, 10.1111/j.1751-908X.2011.00120.x, 2011.
- Kennett, D. J., Breitenbach, S. F., Aquino, V. V., Asmerom, Y., Awe, J., Baldini, J. U., Bartlein, P., Culleton, B. J., Ebert, C., Jazwa, C., Macri, M. J., Marwan, N., Polyak, V., Prufer, K. M., Ridley, H. E., Sodemann, H., Winterhalder, B., and Haug, G. H.: Development and disintegration of Maya political systems in response to climate change, *Science*, 338, 788-791, 695 10.1126/science.1226299, 2012.
- Kennett, D. J., Masson, M., Lope, C. P., Serafin, S., George, R. J., Spencer, T. C., Hoggarth, J. A., Culleton, B. J., Harper, T. K., Prufer, K. M., Milbrath, S., Russell, B. W., González, E. U., McCool, W. C., Aquino, V. V., Paris, E. H., Curtis, J. H., Marwan, N., Zhang, M., Asmerom, Y., Polyak, V. J., Carolin, S. A., James, D. H., Mason, A. J., Henderson, G. M., Brenner, M., Baldini, J. U. L., Breitenbach, S. F. M., and Hodell, D. A.: Drought-Induced Civil Conflict Among the Ancient Maya, 700 *Nature Communications*, 13, 3911, 10.1038/s41467-022-31522-x, 2022.
- Kerber, I. K., Kontor, F., Mielke, A., Warken, S., and Frank, N.: “U–Th Analysis”–open-source software dedicated to MC-ICP-MS U-series data treatment and evaluation, *Geochronology*, 7, 1-13, 2025.
- 695 Kerber, I. K., Arps, J., Eichstädter, R., Kontor, F., Dornick, C., Schröder-Ritzrau, A., Babu, A., Warken, S., and Frank, N.: Simultaneous U and Th isotope measurements for U-series dating using MCICPMS, *Nuclear Instruments and Methods in Physics Research Section B: Beam Interactions with Materials and Atoms*, 539, 169-178, 705 <https://doi.org/10.1016/j.nimb.2023.04.003>, 2023.
- Kotov, S. and Pälke, H.: QAnalySeries-a cross-platform time series tuning and analysis tool, AGU Fall Meeting Abstracts, PP53D-1230,
- 710 Kromer, B., Lindauer, S., Synal, H.-A., and Wacker, L.: MAMS—a new AMS facility at the Curt-Engelhorn-Centre for Achaemetry, Mannheim, Germany, *Nuclear instruments and methods in physics research Section B: beam interactions with materials and atoms*, 294, 11-13, 2013.
- Li, T.-Y., Wang, X., Chen, C.-J., Tan, M., and Wu, Y.: Testing the initial $^{230}\text{Th}/^{232}\text{Th}$ for “Known Age Carbonate” and its significance for ^{230}Th dating and paleoclimate research, *Quaternary International*, 607, 113-119, 2022.
- 715 Lisiecki, L. E. and Raymo, M. E.: A Pliocene-Pleistocene stack of 57 globally distributed benthic $\delta^{18}\text{O}$ records, *Paleoceanography*, 20, 2005.



- Ludwig, K.: Mathematical–statistical treatment of data and errors for $^{230}\text{Th}/\text{U}$ geochronology, *Reviews in Mineralogy and Geochemistry*, 52, 631-656, 2003.
- Ludwig, K.: Isoplot version 4.15: a geochronological toolkit for microsoft Excel, Berkeley Geochronology Center, Special Publication, 247-270, 2008.
- 720 Ludwig, K. R. and Titterton, D. M.: Calculation of $(^{230}\text{Th}/\text{U})$ Isochrons, Ages, and Errors, *Geochimica Et Cosmochimica Acta*, 58, 5031-5042, Doi 10.1016/0016-7037(94)90229-1, 1994.
- Masson, M. and Lope, C. P.: *Kukulcan's realm: Urban life at Ancient Mayapán*, University Press of Colorado 2014.
- Matos, L., Mienis, F., Wienberg, C., Frank, N., Kwiatkowski, C., Groeneveld, J., Thil, F., Abrantes, F., Cunha, M. R., and Hebbeln, D.: Interglacial occurrence of cold-water corals off Cape Lookout (NW Atlantic): First evidence of the Gulf Stream influence, *Deep-Sea Research Part I-Oceanographic Research Papers*, 105, 158-170, 10.1016/j.dsr.2015.09.003, 2015.
- 725 Medina-Elizalde, M., Polanco-Martínez, J. M., Lases-Hernández, F., Bradley, R., and Burns, S.: Testing the “tropical storm” hypothesis of Yucatan Peninsula climate variability during the Maya Terminal Classic Period, *Quaternary Research*, 86, 111-119, 2016a.
- Medina-Elizalde, M., Burns, S. J., Polanco-Martinez, J. M., Beach, T., Lases-Hernandez, F., Shen, C. C., and Wang, H. C.: High-resolution speleothem record of precipitation from the Yucatan Peninsula spanning the Maya Preclassic Period, *Global and Planetary Change*, 138, 93-102, 10.1016/j.gloplacha.2015.10.003, 2016b.
- Medina-Elizalde, M., Burns, S. J., Lea, D. W., Asmerom, Y., von Gunten, L., Polyak, V., Vuille, M., and Karmalkar, A.: High resolution stalagmite climate record from the Yucatán Peninsula spanning the Maya terminal classic period, *Earth and Planetary Science Letters*, 298, 255-262, 10.1016/j.epsl.2010.08.016, 2010.
- 735 Moore, W. S.: The thorium isotope content of ocean water, *Earth and Planetary Science Letters*, 53, 419-426, 1981.
- Moore, W. S. and Sackett, W. M.: Uranium and thorium series inequilibrium in sea water, *Journal of Geophysical Research*, 69, 5401-5405, 1964.
- Morton, L., Evans, C., Harbottle, G., and Estes, G.: Pedogenic fractionation and bioavailability of uranium and thorium in naturally radioactive spodosols, *Soil Science Society of America Journal*, 65, 1197-1203, 2001.
- 740 Moseley, G. E., Richards, D. A., Smart, P. L., Standish, C. D., Hoffmann, D. L., ten Hove, H., and Vinn, O.: Early–middle Holocene relative sea-level oscillation events recorded in a submerged speleothem from the Yucatán Peninsula, Mexico, *The Holocene*, 25, 1511-1521, 2015.
- Moseley, G. E., Edwards, R. L., Wendt, K. A., Cheng, H., Dublyansky, Y., Lu, Y., Boch, R., and Spotl, C.: Reconciliation of the Devils Hole climate record with orbital forcing, *Science*, 351, 165-168, 10.1126/science.aad4132, 2016.
- 745 Nagra, G., Treble, P. C., Andersen, M. S., Bajo, P., Hellstrom, J., and Baker, A.: Dating stalagmites in mediterranean climates using annual trace element cycles, *Scientific reports*, 7, 1-12, 2017.
- Nascimento, R. C., da Silva, Y. J. A. B., do Nascimento, C. W. A., da Silva, Y. J. A. B., da Silva, R. J. A. B., and Collins, A. L.: Thorium content in soil, water and sediment samples and fluvial sediment-associated transport in a catchment system with a semiarid-coastal interface, Brazil, *Environmental Science and Pollution Research*, 26, 33532-33540, 2019.



- 750 Obrist-Farner, J., Steinman, B. A., Stansell, N. D., and Maurer, J.: Incoherency in Central American hydroclimate proxy records spanning the last millennium, *Paleoceanography and Paleoclimatology*, 38, e2022PA004445, 2023.
- Pälike, H.: QAnalySeries [dataset], <https://doi.org/10.5281/zenodo.10892222>, 2024.
- Partin, J. W., Cobb, K. M., Adkins, J. F., Clark, B., and Fernandez, D. P.: Millennial-scale trends in west Pacific warm pool hydrology since the Last Glacial Maximum, *Nature*, 449, 452-455, [10.1038/nature06164](https://doi.org/10.1038/nature06164), 2007.
- 755 Perrin, C., Prestimonaco, L., Servelle, G., Tilhac, R., Maury, M., and Cabrol, P.: Aragonite–calcite speleothems: identifying original and diagenetic features, *Journal of Sedimentary Research*, 84, 245-269, 2014.
- Reiller, P., Moulin, V., Casanova, F., and Dautel, C.: Retention behaviour of humic substances onto mineral surfaces and consequences upon thorium (IV) mobility: case of iron oxides, *Applied Geochemistry*, 17, 1551-1562, 2002.
- Richards, D. A. and Dorale, J. A.: Uranium-series chronology and environmental applications of speleothems, *Uranium-Series Geochemistry*, 52, 407-460, [Doi 10.2113/0520407](https://doi.org/10.2113/0520407), 2003.
- 760 Ridley, H. E., Asmerom, Y., Baldini, J. U. L., Breitenbach, S. F. M., Aquino, V. V., Pruffer, K. M., Culleton, B. J., Polyak, V., Lechleitner, F. A., Kennett, D. J., Zhang, M. H., Marwan, N., Macpherson, C. G., Baldini, L. M., Xiao, T. Y., Peterkin, J. L., Awe, J., and Haug, G. H.: Aerosol forcing of the position of the intertropical convergence zone since AD 1550, *Nature Geoscience*, 8, 195-200, [10.1038/Ngeo2353](https://doi.org/10.1038/Ngeo2353), 2015.
- 765 Rivera-Collazo, I., Winter, A., Scholz, D., Mangini, A., Miller, T., Kushnir, Y., and Black, D.: Human adaptation strategies to abrupt climate change in Puerto Rico ca. 3.5 ka, *The Holocene*, 25, 627-640, [10.1177/0959683614565951](https://doi.org/10.1177/0959683614565951), 2015.
- Roesch, C. and Rehfeld, K.: AUTOMATISING CONSTRUCTION AND EVALUATION OF AGE-DEPTH MODELS FOR HUNDREDS OF SPELEOTHEMS, 2020.
- Roy-Barman, M. and Pons-Branchu, E.: Improved U–Th dating of carbonates with high initial ^{230}Th using stratigraphical and coevality constraints, *Quaternary Geochronology*, 32, 29-39, [10.1016/j.quageo.2015.12.002](https://doi.org/10.1016/j.quageo.2015.12.002), 2016.
- 770 Scholz, D. and Hoffmann, D.: $^{230}\text{Th}/\text{U}$ -dating of fossil corals and speleothems, *Quat. Sci. J.*, 57, 52, 2008.
- Scholz, D. and Hoffmann, D. L.: StalAge – An algorithm designed for construction of speleothem age models, *Quaternary Geochronology*, 6, 369-382, [10.1016/j.quageo.2011.02.002](https://doi.org/10.1016/j.quageo.2011.02.002), 2011.
- Schorndorf, N.: Soil-Sensitive Proxies in Northeast Yucatán Speleothems Since the Classic Maya Period, 2024.
- 775 Schorndorf, N., Frank, N., Ritter, S. M., Warken, S. F., Scholz, C., Keppler, F., Scholz, D., Weber, M., Aviles Olguin, J., and Stinnesbeck, W.: Mid-to late Holocene sea-level rise recorded in Hells Bells $^{234}\text{U}/^{238}\text{U}$ ratio and geochemical composition, *Scientific Reports*, 13, 10011, 2023.
- Scott, M. R.: Thorium and uranium concentrations and isotope ratios in river sediments, *Earth and Planetary Science Letters*, 4, 245-252, 1968.
- 780 Sengupta, D., Dutt, S., Warken, S. F., Singam, A., Frank, N., Sagwal, S., and Maurya, S.: Climate-change induced human migration and socio-political changes in eastern India during the Meghalayan age, *Palaeogeography, Palaeoclimatology, Palaeoecology*, 667, 112873, 2025.



- Skiba, V. and Fohlmeister, J.: Contemporaneously growing speleothems and their value to decipher in-cave processes—A modelling approach, *Geochimica et Cosmochimica Acta*, 348, 381-396, 2023.
- 785 Smith, C. L., Fairchild, I. J., Spotl, C., Frisia, S., Borsato, A., Moreton, S. G., and Wynn, P. M.: Chronology building using objective identification of annual signals in trace element profiles of stalagmites, *Quaternary Geochronology*, 4, 11-21, 10.1016/j.quageo.2008.06.005, 2009.
- Spötl, C., Mangini, A., Frank, N., Eichstädter, R., and Burns, S. J.: Start of the last interglacial period at 135 ka: Evidence from a high Alpine speleothem, *Geology*, 30, 815-818, Doi 10.1130/0091-7613(2002)030<0815:Sotlip>2.0.Co;2, 2002.
- 790 Steidle, S. D., Warken, S. F., Schorndorf, N., Förstel, J., Schröder-Ritzrau, A., Moseley, G. E., Spötl, C., Aviles, J., Stinnesbeck, W., and Frank, N.: Reconstruction of Middle to Late Quaternary sea level using submerged speleothems from the northeastern Yucatán Peninsula, *Journal of Quaternary Science*, 10.1002/jqs.3365, 2021.
- Steinman, B. A., Stansell, N. D., Mann, M. E., Cooke, C. A., Abbott, M. B., Vuille, M., Bird, B. W., Lachniet, M. S., and Fernandez, A.: Interhemispheric antiphasing of neotropical precipitation during the past millennium, *Proceedings of the National Academy of Sciences*, 119, e2120015119, 2022.
- 795 Stinnesbeck, W., Rennie, S. R., Avilés Olguín, J., Stinnesbeck, S. R., Gonzalez, S., Frank, N., Warken, S., Schorndorf, N., Krenzel, T., and Velázquez Morlet, A.: New evidence for an early settlement of the Yucatán Peninsula, Mexico: The Chan Hol 3 woman and her meaning for the Peopling of the Americas, *Plos one*, 15, e0227984, 2020.
- Sullivan, R. M., van Hengstum, P. J., Wallace, E. J., Coats, S., Donnelly, J. P., Korty, R., Little, S. N., Maas Vargas, M. G., 800 Mejia-Ortiz, L., and Reinhardt, E. G.: Yucatan hurricane activity highlights Common Era tropical cyclone dipole, *Geophysical Research Letters*, 52, e2024GL113940, 2025.
- Synal, H. A., Stocker, M., and Suter, M.: MICADAS: A new compact radiocarbon AMS system, *Nuclear Instruments & Methods in Physics Research Section B-Beam Interactions with Materials and Atoms*, 259, 7-13, 10.1016/j.nimb.2007.01.138, 2007.
- 805 Taylor, S. R. and McLennan, S. M.: *The continental crust: its composition and evolution*, 1985.
- Tec, F.: *Centro de Interpretación Biocultural en Áaktun Kóopo, una Caverna del Complejo Santa Rita, Yucatán, México*, Master, Universidad Autónoma de Yucatán, 2021.
- Therre, S., Pross, L., Friedrich, R., Trussel, M., and Frank, N.: Heidelberg Radiocarbon Lab - Establishing a New Carbon Dioxide Extraction Line for Carbonate Samples, *Radiocarbon*, 63, 915-924, 2021.
- 810 Thomas, C.: *Las Cuevas de Yucatán: No. 1 La Región de Valladolid*, 2011.
- Töchterle, P., Steidle, S. D., Edwards, R. L., Dublyansky, Y., Spötl, C., Li, X., Gunn, J., and Moseley, G. E.: 230 Th/ U isochron dating of cryogenic cave carbonates, *Geochronology*, 4, 617-627, 2022.
- Treble, P. C., Baker, A., Abram, N. J., Hellstrom, J. C., Crawford, J., Gagan, M. K., Borsato, A., Griffiths, A. D., Bajo, P., and 815 Markowska, M.: Ubiquitous karst hydrological control on speleothem oxygen isotope variability in a global study, *Communications Earth & Environment*, 3, 29, 2022.
- Vermeesch, P.: IsoplotR: a free and open toolbox for geochronology, *Geoscience Frontiers*, 9, 1479-1493, doi: 10.1016/j.gsf.2018.04.001, 2018.



- 820 Vieten, R., Warken, S. F., Winter, A., Scholz, D., Zanchettin, D., Black, D., and Lachniet, M.: A Sequence of Abrupt Climate Fluctuations in the Northern Caribbean related to the 8.2 ka event, *The Holocene*, 34, 325-337, [10.1177/09596836231211874](https://doi.org/10.1177/09596836231211874), 2024a.
- Vieten, R., Warken, S. F., Zanchettin, D., Winter, A., Scholz, D., Black, D., Koltai, G., and Spötl, C.: Northeastern Caribbean rainfall variability linked to solar and volcanic forcing, *Paleoceanography and Paleoclimatology*, 39, e2023PA004720, 2024b.
- 825 Warken, S., Schorndorf, N., Stinnesbeck, W., Hennhofer, D., Stinnesbeck, S., Förstel, J., Steidle, S., Olguin, J. A., and Frank, N.: Solar Forcing of Early Holocene Droughts on the Yucatán Peninsula, *Scientific Reports*, 11 (13885), [10.1038/s41598-021-93417-z](https://doi.org/10.1038/s41598-021-93417-z), 2021.
- Warken, S., Vieten, R., Winter, A., Spötl, C., Miller, T., Jochum, K., Schröder-Ritzrau, A., Mangini, A., and Scholz, D.: Persistent link between Caribbean precipitation and Atlantic Ocean circulation during the Last Glacial revealed by a speleothem record from Puerto Rico, [10.1002/essoar.10502676.1](https://doi.org/10.1002/essoar.10502676.1), 2020.
- 830 Warken, S. F., Schmitt, A. K., Scholz, D., Hertwig, A., Weber, M., Mertz-Kraus, R., Reinig, F., Esper, J., and Sigl, M.: Discovery of Laacher See eruption in speleothem record synchronizes Greenland and central European Late Glacial climate change, *Science Advances*, 11, eadt4057, 2025.
- Warken, S. F., Fohlmeister, J., Schröder-Ritzrau, A., Constantin, S., Spötl, C., Gerdes, A., Esper, J., Frank, N., Arps, J., Terente, M., Riechelmann, D. F. C., Mangini, A., and Scholz, D.: Reconstruction of late Holocene autumn/winter precipitation variability in SW Romania from a high-resolution speleothem trace element record, *Earth and Planetary Science Letters*, 499, 122-133, [10.1016/j.epsl.2018.07.027](https://doi.org/10.1016/j.epsl.2018.07.027), 2018.
- 835 Webster, J. W., Brook, G. A., Railsback, L. B., Cheng, H., Edwards, R. L., Alexander, C., and Reeder, P. P.: Stalagmite evidence from Belize indicating significant droughts at the time of Preclassic Abandonment, the Maya Hiatus, and the Classic Maya collapse, *Palaeogeography Palaeoclimatology Palaeoecology*, 250, 1-17, [10.1016/j.palaeo.2007.02.022](https://doi.org/10.1016/j.palaeo.2007.02.022), 2007.
- 840 Wefing, A.-M., Arps, J., Blaser, P., Wienberg, C., Hebbeln, D., and Frank, N.: High precision U-series dating of scleractinian cold-water corals using an automated chromatographic U and Th extraction, *Chemical Geology*, 475, 140-148, [10.1016/j.chemgeo.2017.10.036](https://doi.org/10.1016/j.chemgeo.2017.10.036), 2017.
- Wendt, K. A., Li, X., and Edwards, R. L.: Uranium–thorium dating of speleothems, *Elements: An International Magazine of Mineralogy, Geochemistry, and Petrology*, 17, 87-92, 2021.
- 845 Wenz, S., Scholz, D., Sürmelihindi, G., Passchier, C. W., Jochum, K. P., and Andreae, M. O.: ²³⁰Th/U-dating of carbonate deposits from ancient aqueducts, *Quaternary Geochronology*, 32, 40-52, [10.1016/j.quageo.2015.12.001](https://doi.org/10.1016/j.quageo.2015.12.001), 2016.
- Witschey, W. R. and Brown, C. T.: The electronic atlas of ancient Maya sites, [Mayagis. smv. org](http://Mayagis.smv.org), 2010.
- 850 Wortham, B. E., Banner, J. L., James, E. W., Edwards, R. L., and Loewy, S.: Application of cave monitoring to constrain the value and source of detrital ²³⁰Th/²³²Th in speleothem calcite: Implications for U-series geochronology of speleothems, *Palaeogeography, Palaeoclimatology, Palaeoecology*, 596, 110978, <https://doi.org/10.1016/j.palaeo.2022.110978>, 2022.